AFM Study of Droplet Deposition: The Coffee-Stain Effect with Clay Nanoparticles

Hege Sjeggestad Bjørnsen

Department of Physics — NTNU fall 2006

Abstract

There has lately been an increasing interest in the problem of evaporating droplets. It is very important to understand their physical properties, as many applications and experiments require an accurate prediction of the evolution of a single droplet. Often it is also important to be able to control parameters like size and shape. The physics of droplets also influence many aspects of our everyday life, from inkjetprinting of fine patterns to housepaint.

This project was a study of dried droplets deposited on different kinds of substrates. The droplets initially contained different concentrations of the synthetic smectite clay, Laponite, and the objective was to study the deposited material after the droplets had evaporated.

The first sample contained 1% Laponite solution in demineralised water. A 0.1 μl drop was placed on hydrophobic and hydrophilic glass. The surfaces were scanned with the Atomic Force Microscope (AFM) in contact mode after evaporation in both ambient temperature and at 120°C, and there was also done 1D Power Spectral Density (PSD) analysis.

The other samples had concentrations of 0.1%, 0.2%, 0.5%, 1.0%, 1.5% and 2.0% Laponite in demineralised water. These samples were also deposited on the two substrates (0.1 μl), and evaporated under ambient conditions. The surfaces were then scanned with the AFM in tapping mode, and the surface roughness and PSD was studied.

The evaporation process of an initially 1 μl droplet deposited on hydrophobic glass was also investigated, and the diameter and volume was graphed as a function of time.

During the studies we observed different effects that are influencing the particle distribution, like the coffee-stain effect and the Marangoni effect. There are differences in the results between the different concentrations, deposition surfaces and evaporation conditions. We also observed different results in different parts of the stain.

Preface

My project was carried out at Norwegian University of Science and Technology, NTNU, Department of Physics. The project was in the division of complex materials, and I worked under the supervision of Professor Jon Otto Fossum and Doctor Ahmed Gmira.

During the fall semester of 2006 the intention for my project was to study droplets of a clay solution deposited on a substrate for evaporation. This was done utilising an optical microscope, and an Atomic Force Microscope, AFM, in both contact- and tapping mode. The surfaces were also subject to roughness- and particle distribution studies.

The work has given me a useful insight into practical lab work, and has been a good introduction to the Master's thesis the upcoming semester.

Approaching the deadline, we got information regarding the accuracy of the contact mode of the AFM, and decided to switch to tapping mode. As this was discovered late in the process, we were not able to carry out more than a few experiments in tapping mode.

I would like to thank Professor Jon Otto Fossum for welcoming me into the Complex group, and for letting me work with this exciting project. I would also like to thank Doctor Ahmed Gmira for support, assistance and patience. At last I will thank Jon Sætrom for helping me with the report.

Trondheim, December 20th, 2006 Hege Sjeggestad Bjørnsen

Contents

1 Clay

Clay was among the first materials utilised by man, and has been known to, and used by, humans for thousands of years. Archaeologists have found artifacts dating back to approximately 23,000 BC [6, 18]. The scientific study and resulting applications beyond traditional approaches, however, is a relatively recent discipline, which only has roots back to the mid-1930s [6, 16].

There has been a growing scientific activity in the science of clay with the availability of clean chemistry customised synthetic clays [15, 16]. This multidisciplinary approach is at the border between materials science and colloid science, while the multi-scale approach, which is linking nano-, micro- and macro-scale studies, is a challenge for the future of clay science. As clays and clay materials are abundant, inexpensive and environmentally friendly, they will most likely be known as the materials of the 21st century [6].

Clay minerals are a group of phyllosilicates, a subgroup of the silicates [3, 20, 25]. The particles are platelet shaped, with ~ 1 nm thickness, and a lateral size which varies between a few tenths of nanometers up to a few micron [15, 25]. What part clays from other phyllosilicates is that they may contain various amounts of water, and that they allow more substitution of their cations. When some clays absorb water they expand, as the water fills the spaces between stacked silicate layers [20].

Clays are characterised by a layered structure, where the "unit cell" or layer of clay platelets is made of the connection between tetrahedral and octahedral sheets in three dimensions [25]. The different layers are held together by van der Waal's forces [18].

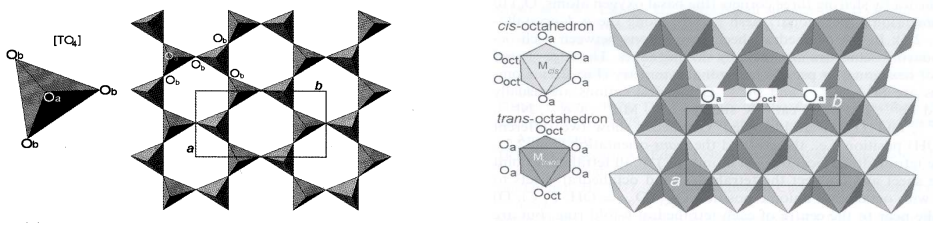

(a) (b)

Figure 1: (a) The tetrahedral sheet is made up of tetrahedra. (b) The octahedral sheet is made up of octahedra. O_a and O_b are referring to the apical and basal oxygen atoms, respectively, while a and b refer to the unit-cell parameters [6].

The continuous two-dimensional tetrahedral sheets consist of e.g. SiO_4, AlO_4 or FeO_4, four oxygen atoms at the corners, and a cation in the middle. All the tetrahedra are linked by sharing three corners of oxygen atoms, while the fourth corner is not shared with another tetrahedron (see Figure 1(a)). The free corners

of all the tetrahedra point in the same direction, and connect the tetrahedral- to an octahedral sheet [3, 6, 25]. The octahedral sheets are made up of octahedra formed from small cations, such as Al^{3+}, Fe^{3+}, Mg^{2+} or Fe^{2+}, coordinated by six oxygen atoms [38]. There is a connection between the octahedra by sharing edges with neighbouring octahedra, and thus forming sheets of hexagonal or pseudo-hexagonal symmetry [6] (see Figure 1(b)). The unshared corner from the tetrahedral sheet also form part of one side of the octahedral sheet. An additional oxygen atom is, however, located above the gap in the tetrahedral sheet at the centre of the six tetrahedra. This oxygen atom is bonded to a hydrogen atom, and thus making up an OH group in the clay structure [38]. Related to the OH position, the octahedra can show two different topologies, the *cis* and the *trans*-orientation [6].

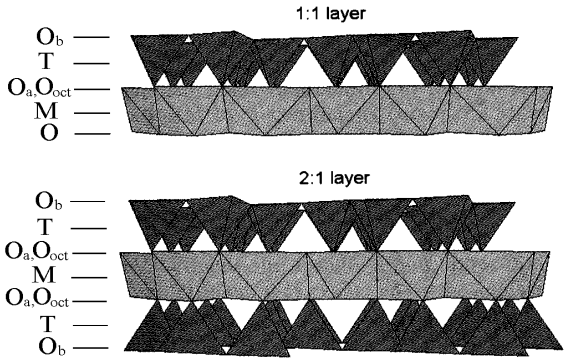

Figure 2: 1:1 and 2:1 layer structure. O_a, O_b and O_{oct} are referring to the tetrahedral apical, tetrahedral basal and the octahedral anionic position, respectively. M and T are the octahedral and tetrahedral cations, respectively [6].

Clays are categorised depending on how the tetrahedral and octahedral sheets make up layers: The 1:1 layer structure consists of the repetition of one tetrahedral and one octahedral sheet in each layer. The unit cell is made up of four tetrahedral sites, and six octahedral sites, four *cis*- and two *trans*-oriented octahedral. The 2:1 layer structure, on the other hand, consists of one octahedral sheet sandwiched between two tetrahedral sheets, with the unshared vertex of each tetrahedral sheet pointing towards the octahedral. Here eight tetrahedral- and six octahedral sites make up the unit cell [6, 25].

The layers can have no charge, or a net negative charge depending on the composition of the tetrahedral and octahedral sheets. In the case of a charged layer, the charge is balanced by interlayer cations like Na^+ or K^+ [38].

2:1 clay minerals are referred to as dioctahedral when four of the six octahedral sites in the unit cell are occupied by cations, while the trioctahedral minerals are those with all six octahedra occupied [6, 25]. This is illustrated in Figure 3.

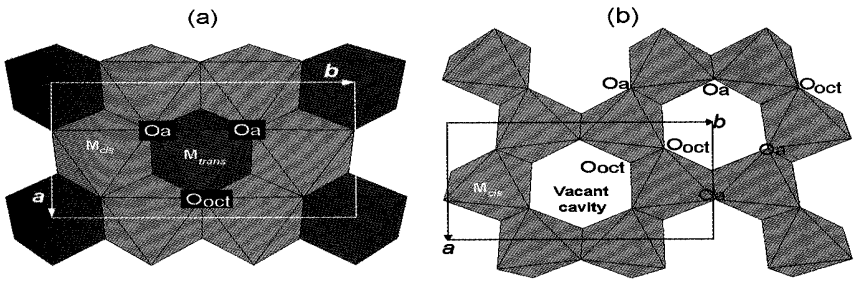

Figure 3: (a) Trioctahedral sheet and (b) dioctahedral sheet. O_a are the apical oxygen atoms shared with tetrahedra, while O_{oct} is the anionic site that is shared between neighbouring octahedra. a and b are the parameters of the unit cell [6].

The dioctahedral smectite has an octahedral sheet dominantly occupied by trivalent cations, while divalent cations dominate the octahedral sheet of trioctahedral smectites.

The general formula for dioctahedral smectites is:

$$(M^{+}_{x+y} \times nH_2O)(R^{3+}_{2-y}R^{2+}_{y})(Si^{4+}_{4-x}Al^{3+}_{x})O_{10}(OH)_2,$$

and that for trioctahedral species is:

$$(M^{+}_{x} \times nH_2O)(R^{2+}_{3-y}R^{3+}_{y})(Si_{4-x-y}Al_{x+y})O_{10}(OH)_2.$$

Here x and y are the layer charge because of the substitutions in tetrahedral and octahedral sites, R^{2+} and R^{3+} are representing the generic divalent and trivalent octahedral cation while M^{+} is the generic monovalent interlayer cation [6].

1.1 Smectites

Smectite clay is a generic name for a 2:1 phyllosilicate, with particles made up of stacks of clay platelets with intercalated balancing cations. The charge density is relatively moderate compared to other 2:1 clay minerals, and is varying between 0.4 e^- and 1.2 e^- per unit cell [6, 25].

A moderate surface charge, like this, is allowing the exchange of intercalated cations with other cations. This charge is allowing penetration of water- or other polar molecules in the interlayer space between the platelets which is causing the smectite grains to swell [25]. Except for the layer charge and the hydration

of the interlayer cations,the structure of smectites is similar to that of other 2:1 phyllosilicates [6].

The mineralogy of smectites that occur naturally are varied and complex, and they are particularly variable chemically. This variation is in part because of the completely undefined interlayer ion position which can be occupied by almost any cation except silicon [35].

1.2 Laponite

Laponite, a synthetic 2:1 trioctahedral hectorite swelling clay, is the most widely studied synthetic clay until now [4, 16]. Its layers are composed of two tetrahedral silica sheets with an octahedral magnesia sheet in between. The chemical composition of Laponite is $Si_8Mg_{5.45}Li_{0,4}H_4O_{24}Na_{0,7}$ (see Figure 4) [4].

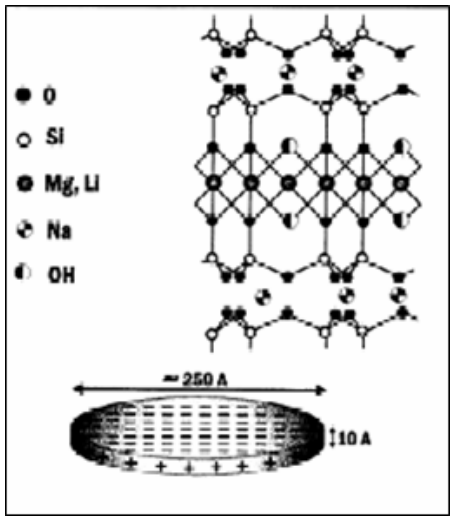

Figure 4: The Laponite structure [8].

Laponite is an interesting clay model system because of its monodispersity and the small particle diameter of about 25 nm. In contrast, natural and other synthetic clays are in general polydisperse with a diameter of a few microns. With a thickness of only 1 nm, the platelets may individually be thought of as single crystals (see Figure 5) [8, 15, 16].

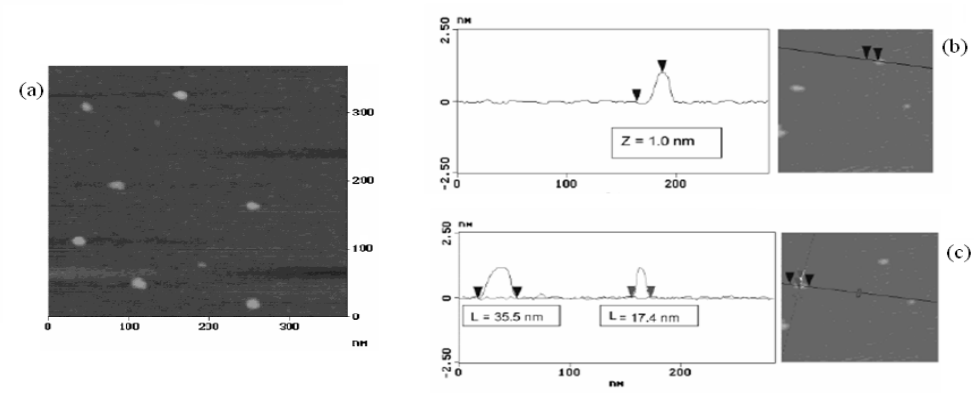

Figure 5: Laponite particles imaged with an atomic force microscope. (a) Isolated Laponite particles. The thickness of the Laponite particle (b) is 1 nm, and the diameter (c) is between 17 and 36 nm [4].

The Laponite particles have a structural negative charge. This charge is balanced by Na^+ counter ions which are located around the particles [4].

The two most common ways to utilise Laponite are: As a rheology modifier, added to the formulation of products like surface coatings, household cleaners, personal care products and other water borne products. It can also be used as a film former, to produce electrically conductive, antistatic and barrier coatings.

There are four fundamental phases, identified experimentally, that govern the overall behaviour at relatively low particle concentrations in the phase diagram of Laponite:

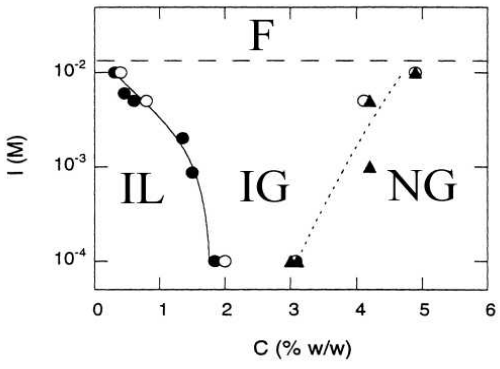

Figure 6: Phase diagram of Laponite, where C is the concentration of Laponite in units of weight percent in water and NaCl, and I is the concentration of NaCl in units of mol/l [23].

First an isotropic liquid (IL) phase which consists of suspended aggregates of primary clay particles. Then, an isotropic gel (IG) phase is observed, where percolating aggregation with fractal properties both dependent on salt-clay concentration and on time. Third, a nematic gel (NG) phase occur, for which excluded volume particle alignment has been proposed. There is also a flocculated (F) phase at high electrolyte concentrations (see Figure 6) [15, 16].

1.3 Applications

When mixed with limited amounts of water, clays become plastic and are then easy to shape. As the clay dries, it becomes firm, and will retain this shape. When clay is exposed to temperatures above 500°C, irreversible chemical reactions begin to take place which makes it hard and water-resistant [18]. These properties are making clays ideal substances for making durable pottery items. With different clay types and different drying conditions, clay has become absolutely necessary to our modern lives. It is the material of different kinds of ceramics, such as earthenware, bricks, porcelain and sanitary ware [6, 37]. Clays can also be used in many industrial processes which include cement production, chemical filtering, oil well drilling and construction [20, 37], and one can find it in paper, plastics, paints, rubber and cosmetics. In addition it has a great importance to crop production, as clays are an important component of soils [6, 16, 20].

2 The physics of droplets

The physics of fluids is playing an important role in many areas of science. For the past few years there has been a lot of research concentrated on micro-scale flows, where the usual laws of hydrodynamics break down [30]. The hydrodynamical laws are no longer valid because the continuum theory only considers macroscopic quantities [19].

The basic entity of a microfluidic system is the *droplet*. Understanding the physical properties of a single droplet is very important, as most applications and experiments require an accurate prediction of the evolution of the size and shape of a droplet. In many applications one also needs to be able to control these parameters. The influence of surface tension, of the viscosity of the liquid, the interaction of the droplet with the substrate, the impact of a droplet on a solid are all examples of the many experiments that can give interesting information of the physics of droplets. The complexity of such systems comes down to the competition between surface effects and bulk properties. For a droplet, interfacial forces, like surface tension and van der Waal's forces, play an important role [30].

There has lately been attracted a great deal of attention to the seemingly simple problem of evaporating droplets. The two situations that have been studied most are droplets deposited on a rough substrate where the contact line remains pinned during the evaporation, and droplets of completely wetting liquids deposited on a perfectly smooth and wetting surface where no anchoring of the contact line occurs [27]. It will here be focused on the first case, where two main effects take part in the droplet's evaporation process:
The first is the "coffee-stain effect", where virtually all the solute may end up on the edge. The second is temperature-gradient-induced Marangoni-Bénard convection, which results in irregular patterns due to an upward flow of the warmer lower liquid [39].

2.1 The Coffee-Stain Effect

The ring shaped residue left when a spilled drop of coffee evaporates on a solid surface, is usually darkest, and thus most concentrated, along the perimeter. The coffee, which initially was dispersed over the entire droplet, now becomes concentrated into a tiny fraction of it [10]. This ring formation is due to a hydrodynamic process, called the coffee-stain effect, where solids (coffee powder) dispersed in the drop are advected to the contact line [9]. The ring-like stains are not particular to coffee but a general phenomenon for any sessile droplet containing solid constituents [11, 40].

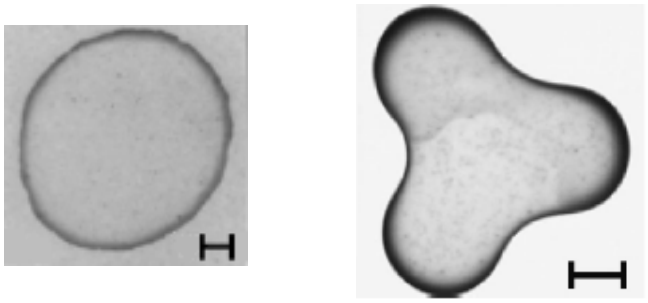

(a) (b)

Figure 7: (a) Normal ring shaped coffee-stain. (b) Manipulated coffee-stain. The drop is darkest at the extremities because of a larger evaporation surface [11].

Two main mechanisms are responsible for the coffee-stain effect: Contact line pinning and predominant evaporation at the edge of the droplet [11]. Because the evaporation rate in a pinned drop is greatest at the edge, the evaporated liquid has to be replenished by a convective flow of liquid from the interior to maintain an equilibrium droplet shape with a fixed boundary. The resulting outward flow may transfer 100% of the solute to the edge, see Figure 8 [11, 28].

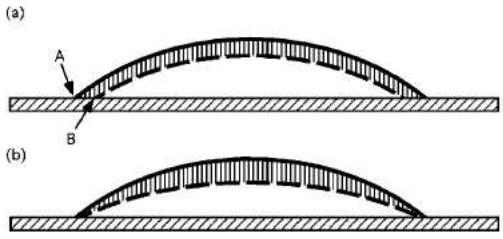

Figure 8: Origin of the advective current. (a) A uniform evaporation is removing the hashed layer for droplets without a pinned contact line. The interface is then moving from the solid line to the dashed line, and the contact line from A to B. However, this movement of the contact line is prevented by pinning (b), and a resulting outward flow is replenishing the evaporated liquid [11].

Deegan and his coworkers have come up with a theory that is predicting the flow velocity, the rate of growth of the ring and the distribution of solute within the drop [11]. As there is a conservation of fluid inside the drop, it is possible to determine the relationship between vertically averaged radial flow of fluid v, the height of the droplet, h, and the rate of liquid loss per unit surface area per unit time from the drop by evaporation, J_s (see Figure 9) [11].

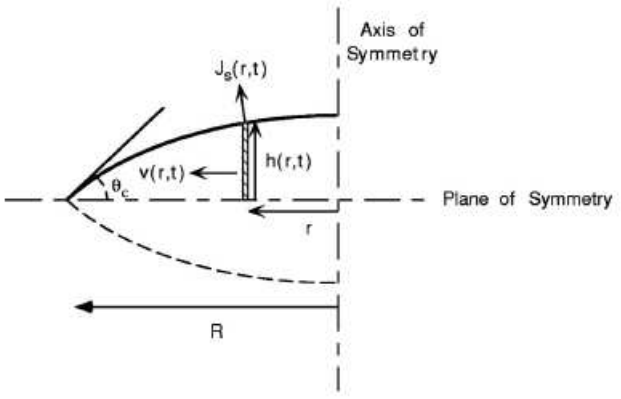

Figure 9: Half a drop viewed from the side. The schematic shows the relevant parameters for the theory [11].

The rate of change of fluid in an infinitesimal annular element at a distance r from the centre of the drop equals the net flux of liquid into the column minus the amount of fluid evaporated from the surface of the element:

$$\rho\frac{\partial h}{\partial t} = -\rho\frac{1}{r}\frac{\partial}{\partial r}(rhv) - J_s(r,t)\sqrt{1+\left(\frac{\partial h}{\partial r}\right)^2}, \tag{1}$$

where t is time and ρ is the density of the liquid.

By rewriting this equation on integral form the equation v is found:

$$v(r,t) = -\frac{1}{\rho r h}\int_0^r \mathrm{d}r r\left(J_s(r,t)\sqrt{1+\left(\frac{\partial h}{\partial r}\right)^2} + \rho\frac{\partial h}{\partial t}\right). \tag{2}$$

By assuming that the droplet is shaped like a spherical cap (see Figure 9), the height can be found by:

$$h(r,t) = \sqrt{\left[\frac{h(0,t)^2+R^2}{2h(0,t)}\right]^2 - r^2} - \frac{R^2-h(0,t)^2}{2h(0,t)}, \tag{3}$$

where R is the radius of the droplet's base, and $h(0,t)$ is the height at the centre.

J_s is depending on whether the rate-limiting step is the transfer rate across the liquid-vapour interface, which means that J_s is a constant, or the diffusive relaxation of the saturated vapour layer immediately above the drop, which means that J_s is strongly enhanced close to the edge of the drop. When the diffusion of the liquid vapour is the limiting rate, it is assumed that a steady state for the evaporation of the drop is quickly achieved, in such a way that the diffusion equation is reduced to Laplace's equation:

$$\nabla^2 u = D\partial_t u \simeq 0. \tag{4}$$

Here D is the diffusion constant for vapour in air and u is the mass of vapour per unit volume of air.

The boundary conditions are (1) that the air is saturated with vapour along the surface of the drop ($u = u_s$), (2) because vapour cannot penetrate the substrate the current normal to the substrate is zero, and (3) far from the drop there is ambient vapour concentrations ($u = u_\infty$).

As the evaporation current is diverging close to the contact line of the drop, J_s can be found by

$$J_s(r,t) \sim (R-r)^{-\lambda}, \tag{5}$$

Here $\lambda = (\pi - 2\theta_c)/(2\pi - 2\theta_c)$ and θ_c is the contact angle at the edge of the droplet.

$$J_s(r,t) \approx J_0 f(\lambda) \left[1 - (r/R)^2\right]^{-\lambda} \tag{6}$$

is a very good approximation to the analytic solution to the boundary value problem.

As can be seen from Eqs. (2) and (5) the velocity is diverging close to the edge of the drop and in the end of the drying time. This means that the change of volume of the wedge near the edge is increasingly getting smaller when approaching the contact line. Therefore the outgoing vapour must be matched by a flow of liquid which is of the same magnitude as the evaporated liquid [11].

Deegan et al. also believe that the drop is self-pinning. The initial roughness or chemical heterogeneities of the substrate are providing a foothold where the contact line first sticks. As there is an accumulation of material at the edge the pinning is strengthened, and eventually this takes over as the primary source of pinning [11].

Sometimes, when a suspension droplet dries on a solid surface, a striped pattern of particles is left behind on the substrate instead of a concentric ring pattern. Adachi et al. observed that the contact line of the droplet was moving towards the centre of the droplet in an oscillatory motion, which was causing a particle-array film at the contact line. They claimed that a "stick-slip" motion was causing this decreasing motion of the droplet [1]. An object which is undergoing stick-slip motion is periodically converting kinetic and internal energy into thermal energy. The coupling of the friction at the contact surface with the object motion is given as the reason for this periodic energy dispersion. In addition, this is accompanying the discharges of suspended particles from the inside to the boundary. The flow to the boundary is causing the particles to assemble and form particle-array films at the contact line. This process is called convective self-assembly of the particles [1].

2.2 The Marangoni Effect

Hu and Larson show that the formation of coffee ring deposits not only requires a pinned contact line, but also suppression of the so called Marangoni flow. For interfaces clean of surfactants, the Marangoni flow reverses the coffee-ring phenomenon and produces deposition at the droplet centre rather than the edge [17].

Since the pioneering studies of Thomson (1855), Marangoni (1865) and Bénard (1900), there has been a lot of attention devoted to what we now know as Marangoni instabilities [29]. As the droplet is evaporating, its surface temperature is reduced non-uniformly. This nonuniform cooling is producing a temperature gradient that leads to a surface tension gradient decreasing with rising temperature. The temperature at the liquid-air surface at the apex of the droplet ought to be the lowest due to a longer thermal conduction path, and because the surface tension is highest there. This is in turn inducing a radially inward Marangoni flow near the droplet surface, that is shown to carry particles that are near the free liquid surface of the droplet from the edge towards the top of the droplet and then plunge them downward to adsorb onto the substrate or be carried along the substrate back to the edge. Here they are recirculated along the free surface back toward the top of the droplet [17]. In other words the Marangoni effects are flows driven by surface tension gradients if the temperature within the droplet is nonuniform [27]. The effect is, however, weak for water droplets [17].

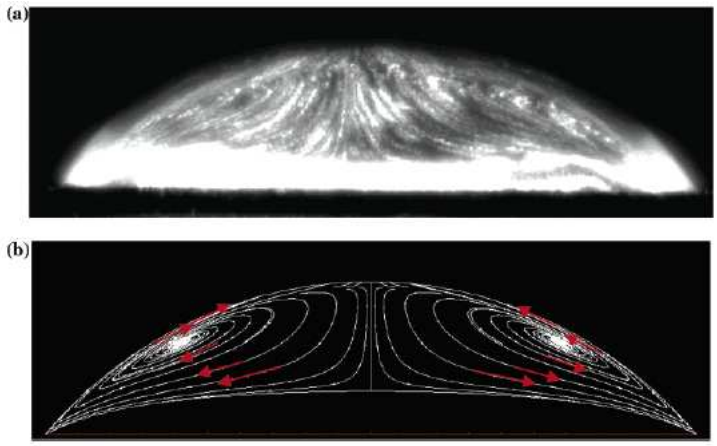

Figure 10: The flow field in an evaporating octane droplet, (a) experimentally and (b) predicted [17].

2.3 Applications

The formation of edge stains is receiving increased attention not only due to the importance from a fundamental point of view, but also because of the relevance in different scientific and industrial applications [40]. Ring deposits are commonplace wherever drops, containing dispersed solids, evaporate on a sur-

face. They may for example influence printing, washing and coating processes. Controlling the distribution of solute during drying may therefore be crucial in many processes [10, 11]. For the manufacture of novel electronics, for instance, dense nanoparticle fluid suspensions are used to inkjet complex patterns, which thus are dried to drive off the suspending medium, and leave a solid thin-film deposit to be used as electronic fixture [40]. The coffee-stain phenomenon is also important in the deposition of DNA/RNA microarrays, spotting methods for gene mapping and drug discovery [17]. In other cases, however, the segregation effects are undesirable and the paint manufacturers, for example, use a variety of additives to ensure that the pigment is evenly dispersed and remains so during drying [11].

3 AFM

The Atomic Force Microscope (AFM) was invented in 1986 by Binnig, Quate and Gerber, and it is today one of the leading tools of imaging, measuring and manipulating matter at nanoscale [36]. It is a type of Scanning Probe Microscopy (SPM), which makes use of the small forces that can be found between materials in close proximity to the surface. AFM can therefore be applied to all kinds of materials, conducting, semiconducting and insulating [26].

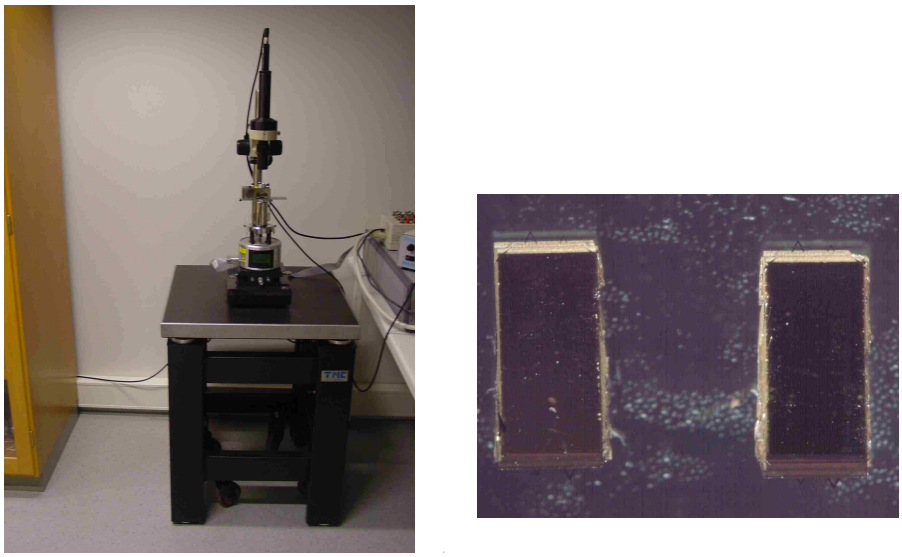

(a) (b)

Figure 11: (a) The MultiMode^{TM} Atomic Force Microscope on top of a vibration insulator. (b) Silicon nitride cantilever probes used for contact mode AFM.

The AFM is utilising a micro scale cantilever, usually made of silicon or silicon nitride (see Figure 11), with a sharp tip at its end that is scanning the surface of the sample. The tip is placed very close to the surface, and attractive and repulsive forces between tip and sample are leading to a deflection of the cantilever [36]. The deflection is measured by a laser spot reflected from the top of the cantilever into a position-sensitive detector that is made up of two side-by-side photodiodes. The difference between the signals from the two photodiodes is indicating the position of the laser spot on the detector, and thus the angular deflection of the cantilever [5]. This is shown in Figure 12. The AFM pictures can be presented by means of either height, deflection or friction.

To maintain a contact force, a feedback mechanism is adjusting the distance between tip and surface. For this purpose the sample is mounted on a piezoelectric tube, which can move the sample in the z-direction. It also moves in the x- and y-directions, and the result is a map of $s(x, y)$ which is representing the topography of the sample [36].

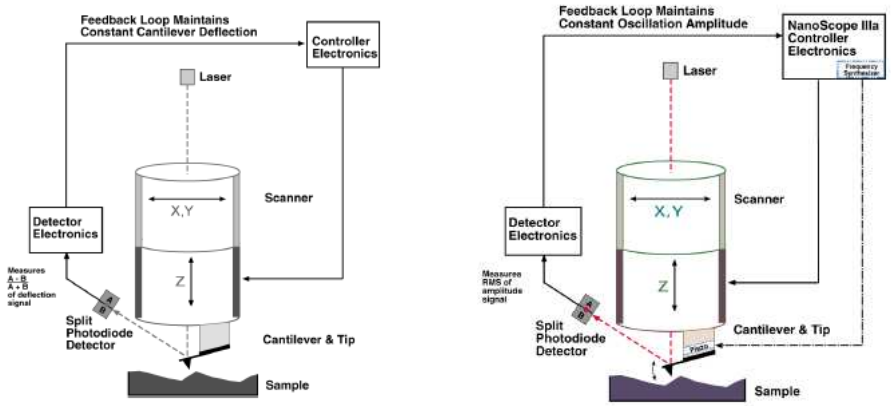

(a) (b)

Figure 12: (a) The feedback loop is maintaining constant cantilever deflection in Contact Mode. (b) Feedback loop electronics in Tapping Mode [33].

There are primary two modes of Atomic Force Microscopy: contact mode and tapping mode. In contact mode the cantilever tip is scanned across the sample surface while the tip is in actual contact with the surface. The change in cantilever deflection is monitored, and thus the surface topology is mapped. The accuracy of the scanning corresponds to the sharpness of the tip [26]. In tapping mode the probe is carefully oscillating in the z-direction, tapping the surface and thus detecting the surface hardness [26]. The cantilever is oscillating in free air at its resonance frequency. As the cantilever is bouncing vertically, the reflected laser beam is deflected in a regular pattern over a photodiode array, generating a sinusoidal electronic signal [12].

3.1 Resolution

As traditional microscopes use optical lenses they only have one measure of resolution, the resolution in the plane of the image. The resolution of the AFM is limited by the shape of the probe, rather than diffraction effects, and thus has two measures of resolution, the plane of the measurement (lateral(x, y)), and in the direction perpendicular to the surface (vertical(z)). Atomic force microscopy thus becomes a three dimensional imaging technique [5, 24].

Lateral resolution is usually defined as the ability to distinguish two separate points on an image [22]. This resolution depends on the geometry of the probe that is used for scanning. The radius of curvature of the end of the tip is determining the highest lateral resolution that can be obtained with a specific tip. A sharper tip with a small radius of curvature can thus laterally resolve smaller features than a dull tip with a larger radius of curvature, (see Figure 13) [33]. The sharpest tips available commercially can have a radius as small as

50 Å [7]. The sidewall angles of the tip is also determining the ability to probe a high aspect ratio. In addition it is possible, in the software, to choose the number of data points (pixels) present in the image in the x and y direction. It is not possible to resolve features smaller than the pixel size of the image [33].

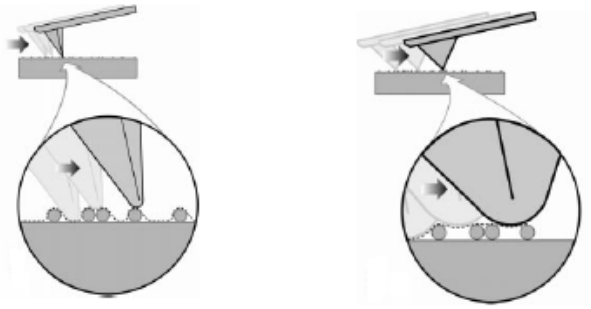

(a) (b)

Figure 13: Surface scanned with (a) a sharp tip and (b) a dull tip. The smaller the radius of curvature, the smaller the resolved features. A sharper tip can laterally resolve smaller features than a dull tip [33].

The resolution in the vertical direction is not determined by the tip shape. Instead it is primarily determined by the resolution of the vertical scanner movement, which is <1 Å. The sidewall angles of the tip determine the AFM's ability to image steep sidewalls on a sample surface, which means that the tip is not able to profile sides of surfaces steeper than the sidewall angle of the tip. This implies that the sidewall angle in the images will reflect the sidewall angle of the tip when scanning across features which are steeper than the tip, as seen in Figure 14. The size of the smallest resolvable height change is limited by the number of pixels in the vertical direction [33].

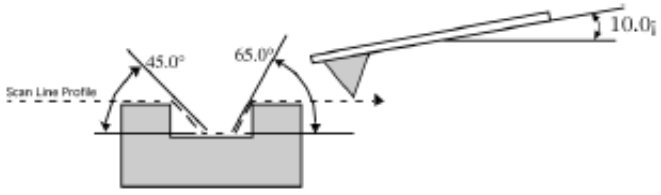

Figure 14: Scanning of features that are steeper than sidewall angle of the tip, the sidewall angle in the image will reflect the sidewall angle of the tip. (Scanning angle from front to back, i.e. scan angle = 0°) [33].

The overall system noise is the largest factor limiting the vertical resolution that can be acquired with the AFM. This may be a result of combined effects from acoustic noise, floor vibrations and thermal vibrations. To get the maximum vertical resolution the vibrations need to be minimised [24]. The AFM is thus placed on a vibration isolator in a room of constant temperature, as seen in Figure 11(a) [33].

The AFM can achieve a resolution of 10 pm, and unlike electron microscopes it can image samples in different environments, such as liquids, vacuum and low temperatures [5].

3.2 The Fluid Cell

Imaging of samples in a fluid is a growing application of the AFM technology. The fluid cell is used to minimise surface forces on delicate samples, the need to observe biological specimens in their natural, fluid environment, or the necessity to make real time observations of samples that are undergoing electrochemical reactions.

The attractive forces due to surface tension are eliminated when imaging samples under fluid. Thus one only need a minimum of cantilever tip force for the sample surface to be imaged. This may be a a decided advantage when imaging biological specimens and delicate materials. The procedure for observing samples under fluid is the same as for contact mode- or tapping mode AFM in air.

The fluid cell is consisting of a small glass assembly with a wire clip for holding the AFM probe. The glass surfaces provide a flat, bevelled interface so that the AFM laser beam may pass into the fluid without being distorted by an unstable fluid surface [13].

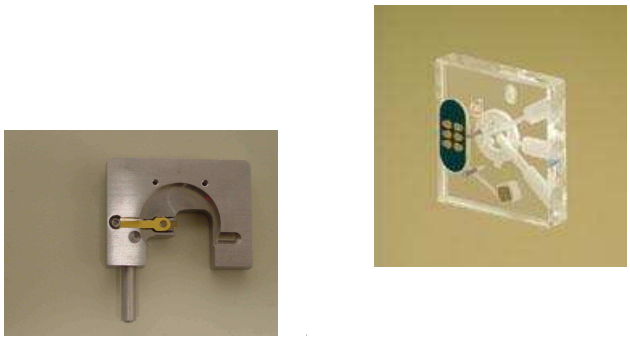

(a) (b)

Figure 15: (a) The cell for normal scanning and (b) the fluid cell [21].

3.3 Surface Roughness

The surface roughness is the measure of the irregularities in the surface texture, and can be found utilising the roughness analysis tool in Nanoscope offline [33]. The roughness statistics that have been used for this project work are:

- **Mean roughness (R_a):** The arithmetic average of the absolute values of the surface height deviations which are measured from the mean plane:

$$R_a = \frac{1}{N}\sum_{j=1}^{N}|Z_j| \tag{7}$$

- **RMS (R_q):** The standard deviation of the Z-value:

$$R_q = \sqrt{\frac{\sum (Z_i)^2}{N}}, \tag{8}$$

  where Z_i is the current Z value, and N the number of points within the area of interest.

- **Maximum height (R_{max}):** Maximum vertical distance between the highest and lowest data points within the area of interest.

- *Zrange*: The peak-to-valley difference in height values within the analysed region [14].

R_{max} and *Zrange* are basically the same.

3.4 Power Spectral Density

When analysing the roughness of a sample surface, the Power Spectral Density (PSD) function is a very useful tool. By using this function you achieve a representation of the amplitude of the surface roughness as a function of spatial frequency of the roughness. Surface features that otherwise might appear random are revealed, and a graphic representation of how the surface features are distributed is provided [32].

The following information can be calculated by the Power Spectral Density function:

- Total power spectrum
- 1D PSD
- 1D isotropic PSD
- 2D isotropic PSD

- RMS roughness values

In this report only the 1D PSD has been used.

Mathematically, the PSD is approximately defined as the frequency distribution for a digitised profile of length L, which consists of N points sampled at intervals of d_0:

$$PSD(f) = \frac{2d_0}{N}\left|\sum_{n=1}^{N} \exp^{\frac{i2\pi}{N}(n-1)(m-1)} z(n)\right|^2 \text{ for } f = \frac{m-1}{Nd_0}. \tag{9}$$

Here $i = \sqrt{-1}$, and the frequencies, f, are ranging from $\frac{1}{L}$ to $\frac{N/2}{L}$. The algorithm used to obtain the PSD is depending on the Fast Fourier Transform (FFT) of the image squared to derive the power, P. The power may then be used to derive the various various PSD-like values:

- 1D PSD = $\frac{P}{\Delta f}$
- 1D isotropic PSD = $\frac{P}{2\pi f}$
- 2D isotropic PSD = $\frac{P}{2\pi f(\Delta f)}$

f and Δf are derived by progressively sampling data from the two-dimensional FFT centre of the image, as seen in Figure 16.

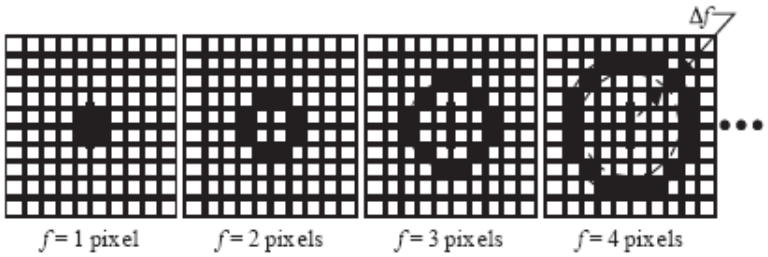

Figure 16: Progressive data sampling [14]

Here each sampling swings a "data bucket" of a given frequency f. The sampling frequency, f, is limited to $\frac{N/2}{L}$ (where N is the scan size in pixels) because samples are taken from the image centre. This is forming the highest frequency of the PSD plot. The lowest frequency is defined at $1/L$ [14].

4 Experiment

4.1 Deposition Surfaces

For the experiments two different substrates were used, normal or hydrophilic glass (wetting) and silanised or hydrophobic glass (non-wetting). To prepare the hydrophobic substrate, the glass had to be treated with a silanisation solution (Assay ~5% dimethyldichlorosilane in heptane, $C_2H_6Cl_2Si$). This was done to avoid the strong attraction of water that is present in normal hydrophilic glass, and that makes the water spread out on the glass surface. The glass was treated by being lowered into the silanisation solution, and it remained there for a few hours. The hydrophilic and hydrophobic surfaces are sketched in Figure 17.

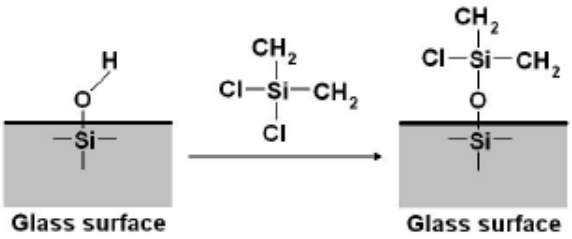

Figure 17: Silanisation of a glass surface with reactive chlorosilane [2].

4.2 Experimental Setup

The AFM images were taken using a MultiMode^{TM} Atomic Force Microscope from Veeco Instruments, operating in normal room air (see Figure 11(a)). This AFM is user friendly, and can easily image on atomic and microscopic scales. The AFM can scan from the maximum scan size of 125 micron to a few nanometers with full 16-bit resolution on all scan waveforms and each axis. The MultiMode AFM has three different scanners for different scan sizes [31]. The A-scanner has a scan size of (0.4×0.4) μm, the E-scanner a size of (10×10) μm and the J-scanner has a size of (125×125) μm. For our purpose the E-scanner was the best choice, as we are only scanning between 2 and 10 μm.

A complete range of AFM techniques for surface characterisation of properties can be performed with this high resolution tool. These include topography, elasticity, friction, adhesion and electrical/magnetic fields. It can also heat and cool samples for biological applications, polymers or other materials, and is able to scan samples in liquids. The MultiMode is today the most widely used AFM in the world [31]. The probes that are used for scanning are NP Series Probes, model NP-20 from Veeco for contact mode, and Tap300 Metrology Probes, model RTESP7 for tapping mode [34]. See Appendix B for details.

Figure 18: The three scanners for the MultiMode AFM, J, E and A.

The number of data points present in the image are restricted to 512, 256 and 128 for the MultiMode AFM [33]. To get representative images, several 10×10 μm and 2×2 μm square areas were imaged with a resolution of 256 data points per line, for both contact- and tapping mode.

4.3 Sample 1

For the first sample, 1 g of Laponite RDS particles (see Appendix A) was mixed with 100 ml of demineralised water. This solution was stirred with the magnetic stirrer for a few hours, until it was thoroughly mixed. The dispersion was then filtered through a filter with pores of size 0.2 μm. This was done to remove the larger agglomerates that otherwise would disturb the results. A pipette was used to place 0.1 μl droplet on hydrophilic and hydrophobic glass. There were two samples on hydrophilic glass and two samples on hydrophobic glass. One of each was dried under ambient conditions, and the other two were placed in an oven at 120°C for 15 minutes.

4.3.1 Macroscopical Study

The purpose of the macroscopical study was to study the morphology, size and shape of the droplets, disposed on different substrates and evaporated under different conditions. This was done by using an optical microscope. The samples that evaporated at room temperature were studied with the optical microscope as they dried. The other two were studied after the heating.

4.3.2 Microscopical Study

For the microscopical study the droplets were scanned with the AFM contact mode to characterise the surface. Four locations at the ring edge, four in the interior and one in the middle. For all the locations 10x10 and 2x2 μm scans were used. The particle distribution in different locations of the droplets were

studied with help from the PSD-tool in Nanoscope offline. The 1D PSD-data was then plotted as a function of length scale.

4.4 Samples 2 - 7

Samples with 0.1, 0.2, 0.5, 1.0, 1.5 and 2.0 g of Laponite RD (see Appendix A) were prepared in 100 ml of demineralised water, to get concentrations of 0.1, 0.2, 0.5, 1.0, 1.5 and 2.0% respectively. The solutions were then stirred on the magnetic stirrer for a few hours, before they were filtered through filter paper of poresize 0.2 μm. The 1.0, 1.5 and 2.0% samples, however, were too concentrated to filter, and therefore left unfiltered. Droplets of size 0.1 μl were then placed on hydrophilic- and hydrophobic glass. The different samples were studied with the AFM in tapping mode.

4.4.1 Microscopical Study

For the microscopical study the AFM was used to characterise the surfaces of the evaporated droplets. The different concentrations were compared, and the edge-thickness for the samples were measured. The roughness of the inside of the drops was calculated, and we also did a 1D PSD analysis of the data.

4.4.2 Macroscopical Study

A 1 μl droplet of concentration 0.2% was placed on a hydrophobic surface on top of a balance, and the weight was measured as the droplet evaporated. The weight was then graphed as a function of time.

To compare the volume with the diameter another 1 μl droplet was deposited on hydrophobic glass, but this time under an optical microscope. Pictures were taken every 20 seconds during the evaporation. A millimetre paper was used as a scale. To minimise effects on the evaporation process, a light source of low intensity was used.

5 Results and Discussion

5.1 Surface Comparison

To analyse the results correctly it was important to compare the different clean substrates. The surfaces without droplets were thus scanned, and then the roughnesses and heights were measured. The results are shown in Figure 19 and Table 1.

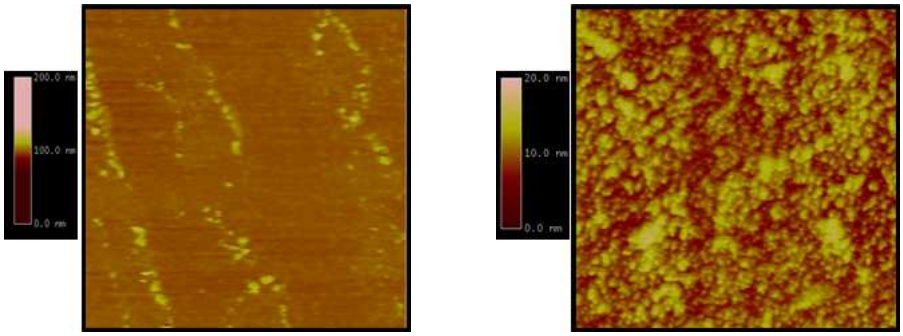

(a) (b)

Figure 19: Comparison of droplets on (a) hydrophilic glass and (b) hydrophobic glass.

Table 1: Surface Comparison

Substrate	RMS (R_q)	Mean roughness (R_a)	Max height ($R_{max}/Zrange$)
Normal glass	2.47 nm	1.13 nm	65.75 nm
Silanised glass	1.92 nm	1.6 nm	13 nm

5.2 Sample 1

5.2.1 Macroscopical Results

Hydrophobic Glass: The droplet on hydrophobic glass remains spherical, and without a contact line for a few minutes of the evaporation process (see Figure 20). Because the contact line is not pinned, the diameter is decreasing until the sphere is collapsing (after 2.5 minutes in Figure 20). When the droplet has collapsed, the decreasing stops and the edge is remaining in the same position, like a pinned contact line for droplets on wetting surfaces.

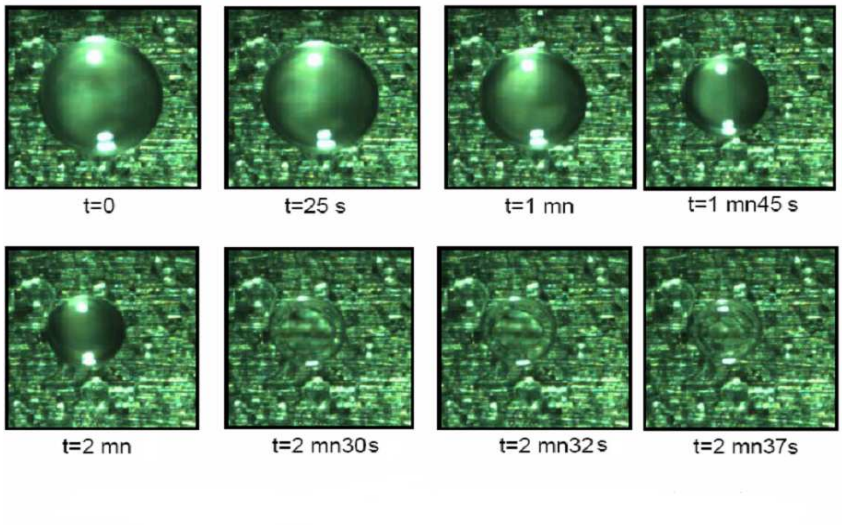

Figure 20: The evolution of an evaporating droplet on hydrophobic glass.

Hydrophilic Glass: Because the hydrophilic glass means that it is wetting, the droplet is spreading out as soon as it is deposited on the surface. The contact line is pinned after a few seconds, and the droplets evolution is according to the coffee-stain effect. This means that the droplet has the same diameter throughout the evaporation process.

As seen in Figure 21(b), the droplet on the hydrophobic glass ends up as a stain with a well defined thick edge. The diameter of the stain is about 165 μm, and the edge thickness about 26 μm. It is harder to distinguish the edge for the droplet on the hydrophilic glass, as it is much less clear than for the hydrophobic case. Through the optical microscope we could see a smooth and thin ring with a diameter of about 600 μm (Figure 21(a)).

Heated Samples: For the samples that were heated at 120°C, the pictures from the optical microscope show that the droplets might be influenced by the stick-slip motion explained in Section 2.1 (Figure 22). The droplet on the

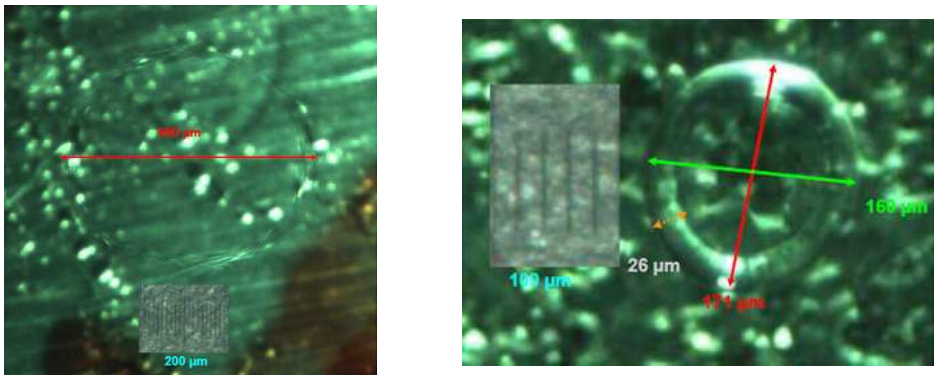

(a) (b)

Figure 21: Comparison of droplets on (a) hydrophilic glass and (b) hydrophobic glass.

hydrophilic surface has a pattern of concentric rings inside the edge. The droplet on the hydrophobic surface on the other hand has a more "messy" pattern. The diameter of the hydrophobic droplet is about 300 μm, while the diameter of the hydrophilic droplet is 530 μm.

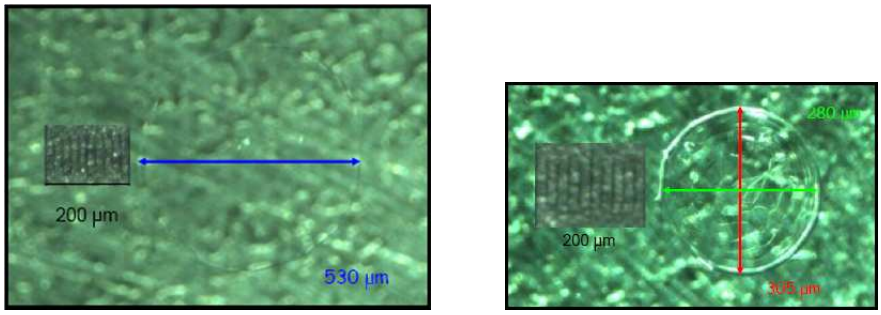

(a) (b)

Figure 22: Heated droplets on (a) hydrophilic glass and (b) hydrophobic glass.

The fact that the diameter of the heated droplet on hydrophobic glass is about 100 μm larger than for the non-heated droplet might be due to an earlier collapse because of the heat. The diameter of the droplet on hydrophilic glass is about the same as for the non-heated. It is, however, a little smaller as the contact line is pinned earlier because of the faster evaporation.

5.2.2 Microscopical Results

As seen in Figure 23 the tendencies of the particle distribution on the two substrates are the same. The dimensions are, however, very different. For the droplet on hydrophilic glass the maximum height is 700 nm, while the maximum height for the droplet on hydrophobic glass is 2500 nm. Inside the ring the maximum height of the droplet on hydrophilic glass is 200 nm, while it for the hydrophobic glass only is 100 nm. It is evident from the pictures that the droplet on hydrophobic glass has a better ability to carry the solute to the edge.

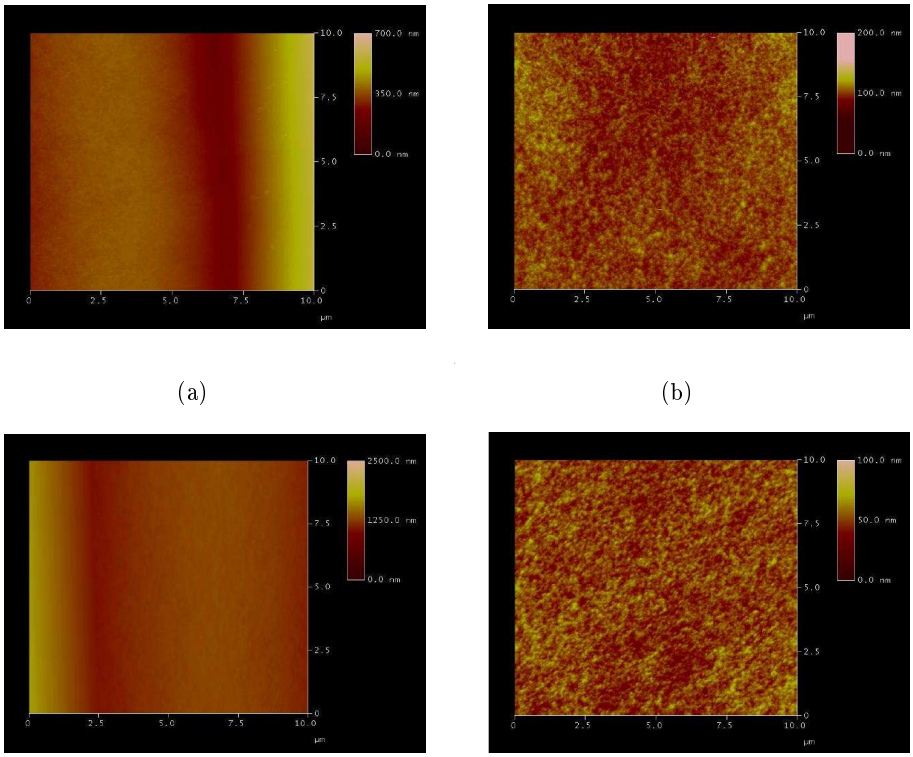

Figure 23: Droplets on hydrophilic- ((a) and (b)), and hydrophobic ((c) and (d)) glass. The samples are scanned on the edge ((a) and (c)), and on the inside ((b) and (d)).

Marangoni Effect: In contrast to the relatively smooth pattern found in other spots inside the ring, the pattern in the middle of both the drop on hydrophilic- and the one on hydrophobic glass is characterised by large and distinct agglomerates (see Figure 24). As explained in Section 2.2 the effect which makes the liquid carry the particles towards the top of the droplet and plunge them downward to adsorb onto the substrate, is known as the Marangoni effect [17]. For the Marangoni effect we get a strong pattern in the middle of the stain instead of, or in addition to, the concentrated ring for the coffee-stain effect. With the agglomeration in Figure 24 it is reason to believe that the Marangoni effect is present in our droplets.

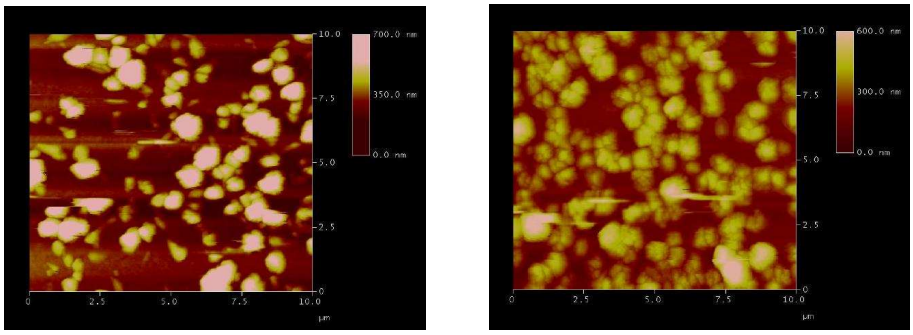

(a) (b)

Figure 24: Possible Marangoni effect in droplets on (a) hydrophilic and (b) hydrophobic glass.

1D PSD Analysis: For the 1D PSD of the hydrophilic surface the graphs turned out as in Figure 25. The x- and y-data are almost the same for the inside of the ring and on the edge. We got the same results for the hydrophobic surface (Figure 26).

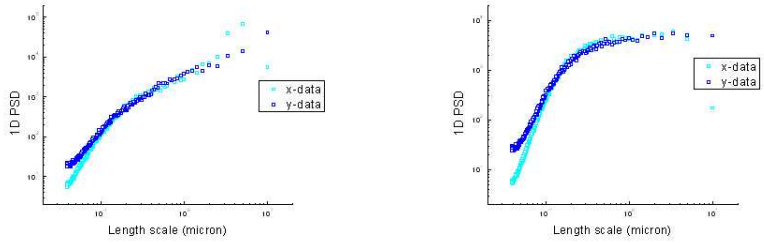

(a) (b)

Figure 25: 1D PSD for the droplet on hydrophilic glass, scanned (a) on the edge, and (b) on the inside.

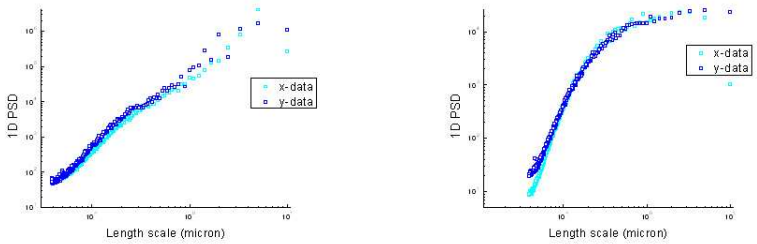

(a) (b)

Figure 26: 1D PSD for the droplet on hydrophobic glass, scanned (a) on the edge, and (b) on the inside.

Heated Samples: Microscopically there is a large difference between the hydrophilic and hydrophobic glass for the droplets dried at 120°C. As seen in Figure 27 the droplets on hydrophilic glass have lots of agglomeration both on the edge and on the inside of the ring. The height at the edge has the same value as for non-heated samples, but inside the ring the maximum height is 400 nm as opposed to 200 nm. This agrees with the results from the macroscopical analysis, and strengthens the assumption about the stick-slip motion. For the middle of the droplet the agglomerates seem larger than in the rest of the drop (see Figure 28). This might be an indication that the Marangoni effect also is present in heated droplets.

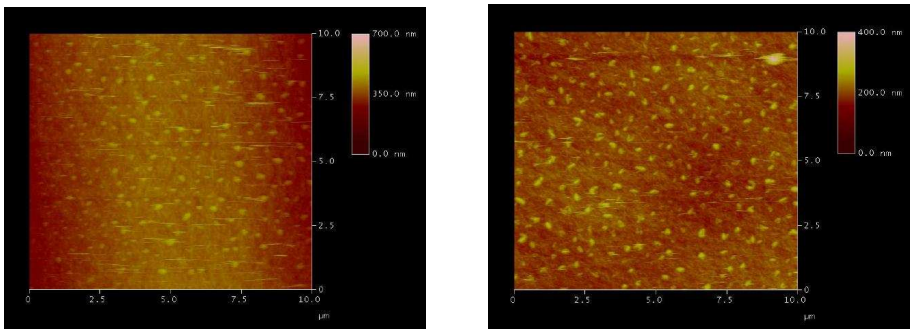

(a) (b)

Figure 27: Droplet on hydrophilic glass heated at 120°C. Scanned (a) on the edge, (b) on the inside.

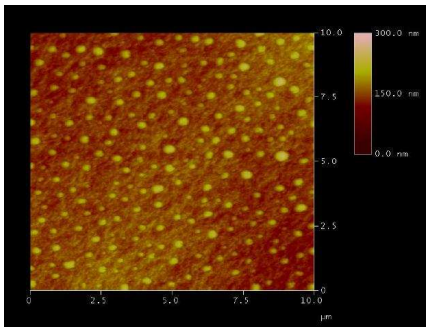

Figure 28: Droplet on hydrophilic glass heated at 120°C, and scanned in the middle.

The height of the edge of the droplet on hydrophobic glass is much smaller for the heated sample ($\sim$ 1000 nm) than for the sample dried in ambient temperature ($\sim$ 2500 nm) (Figure 29). It is thus evident that the coffee stain effect is stronger for the non-heated samples. The maximum height of the inside is 800 nm which might be due to a stripe-pattern because of stick-slip motion. The pattern is more evident for the friction scan than for the height scan, as is shown in Figure 30.

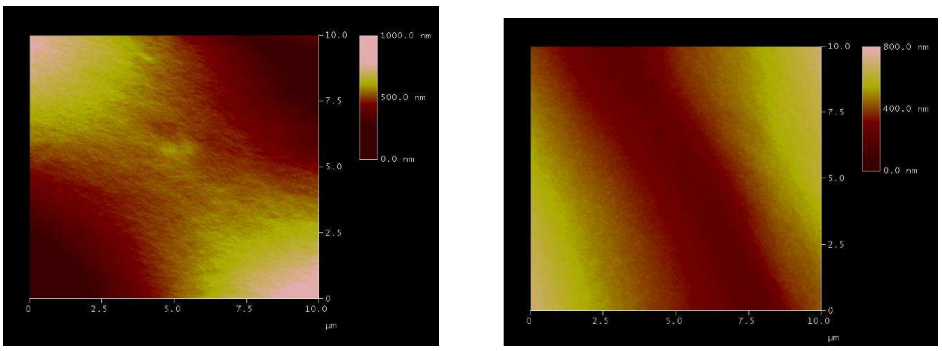

(a) (b)

Figure 29: Droplet on hydrophobic glass heated at 120°C. Scanned (a) on the edge, and (b) on the inside.

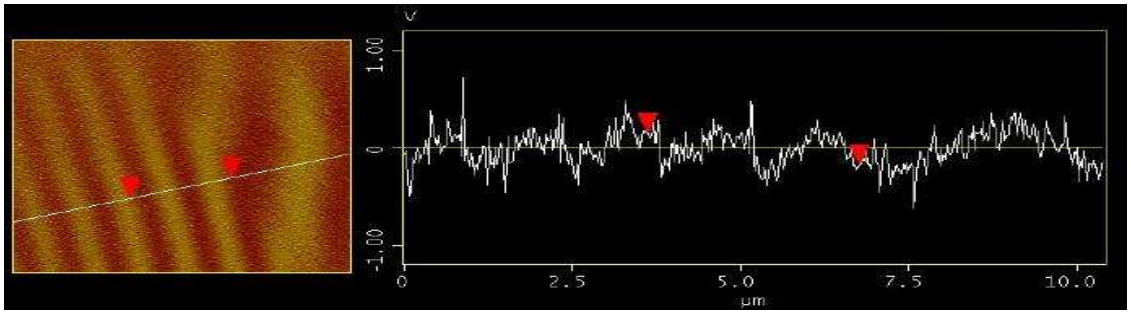

Figure 30: Stripe pattern possibly due to stick-slip motion. Here the friction is imaged, not the height.

5.3 Samples 2 - 7

5.3.1 Inside the Ring

For samples 2 - 7 the pictures of the different concentrations were compared (Figures 31 and 32). In the hydrophilic pictures we can observe more agglomeration than in the hydrophobic, especially for 0.1% (a), 1.5% (e) and 2.0% (f). There is not much difference between the hydrophobic pictures.

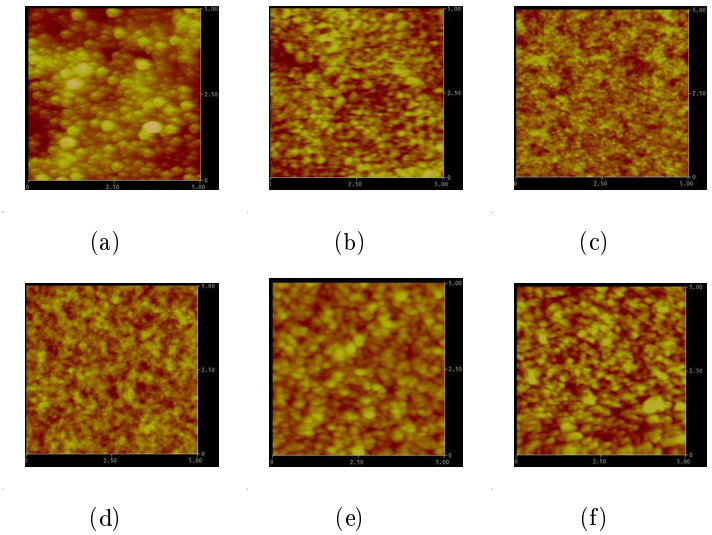

Figure 31: The different concentrations of the solutions on hydrophilic glass. (a) 0.1%, (b) 0.2%, (c) 0.5%, (d) 1.0%, (e) 1.5% and (f) 2.0%.

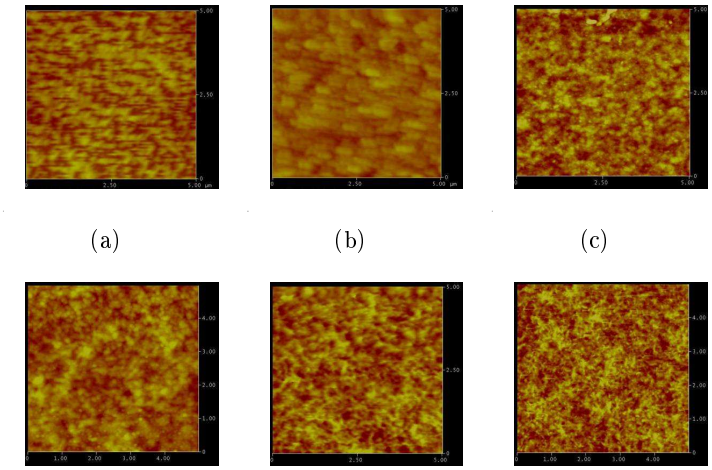

(a) (b) (c)

(d) (e) (f)

Figure 32: The different concentrations of the solutions on hydrophobic glass. (a) 0.1%, (b) 0.2%, (c) 0.5%, (d) 1.0%, (e) 1.5% and (f) 2.0%.

5.3.2 Surface Roughness

For the hydrophilic surface, the roughness inside the ring is not changing much with the dispersion concentration. The average values are $R_q = 7$ nm and $R_a = 6$ nm. For the hydrophobic surface all the laponite suspensions except 0.1% show similar behaviour for the surface roughness inside the ring. The values for the 0.1% suspension are $R_q = 14$ nm and $R_a = 12$ nm), while the average value for the others are $R_q = 7$ nm and $R_a = 6$ nm.

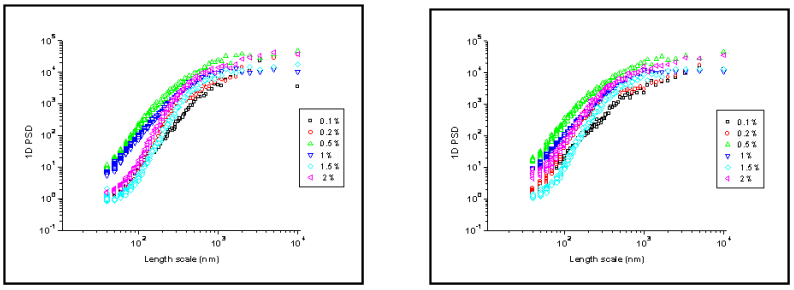

(a) (b)

Figure 33: 1D PSD of the droplets on hydrophilic glass for the different concentrations. ((a) scanned in the x-direction and (b) scanned in the y-direction.)

The 1D PSD of the hydrophilic and hydrophobic samples seem affected by the dispersion concentration. In Figures 33 and 34 it can seem like all the

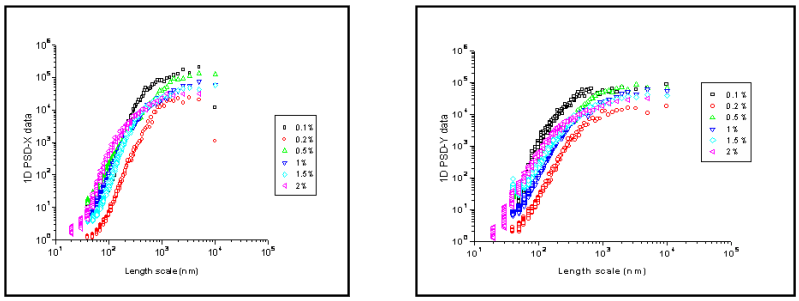

(a) (b)

Figure 34: 1D PSD of the droplets on hydrophobic glass for the different concentrations. ((a) scanned in the x-direction and (b) scanned in the y-direction.)

concentrations have the same behaviour, but with a closer look at the slopes of the different concentrations (Figure 35) it is evident that there is a difference.

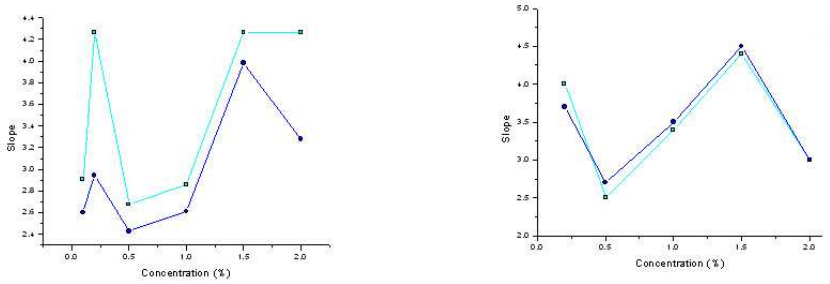

(a) (b)

Figure 35: The slopes as a function of concentration. (a) On hydrophilic glass and (b) on hydrophobic glass. (The turquoise is the x-data, and the blue is the y-data.)

5.3.3 On the Edge

Edge Thickness: It is difficult to measure the thickness of the edge correctly with the optical microscope. For these samples we therefore tried to see the thickness with help from the AFM. For the hydrophilic glass the edge thickness is decreasing with the concentration (see Figure 36), and we get the largest values for 0.1% and 0.2% with 7 μm. The thinnest edge is observed for the 2% solution, with 2 μm.

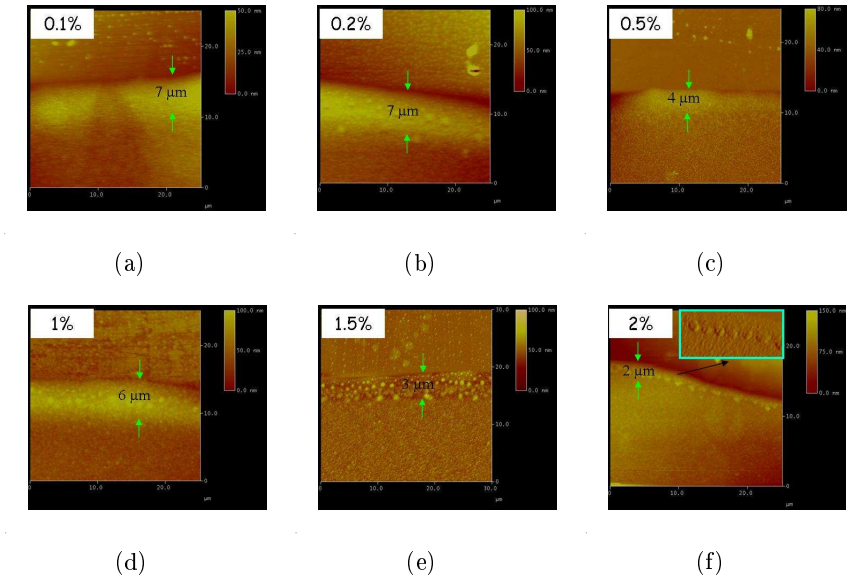

Figure 36: Thickness of the edges for the different concentrations on hydrophilic glass.

As seen in Figure 37, the tendency is the opposite for the hydrophobic surface. It is not easy to distinguish the edge for the 0.1% concentration as it is only 280 nm thick. The edge is a little thicker for the 0.2% solution with a thickness of 1 μm but for the 0.5, 1.0, 1.5 and 2.0% concentrations the edge is thick, and between 7 and 9 μm.

In Figure 38 the different edge thicknesses are plotted as a function of concentration. The tendency for the two substrates is almost opposite. The edge is, however, only scanned in one position, and the results might have turned out differently if more than one spot was scanned.

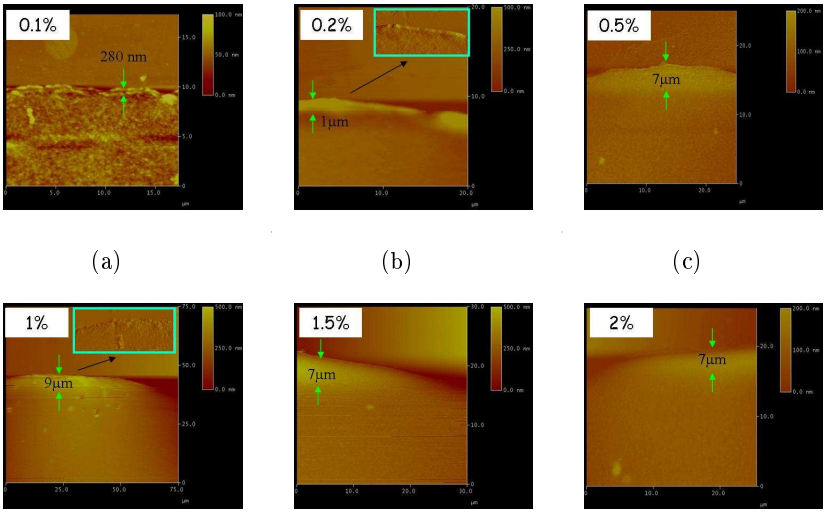

(a) (b) (c)

(d) (e) (f)

Figure 37: Thickness of the edges for the different concentrations on hydrophobic glass.

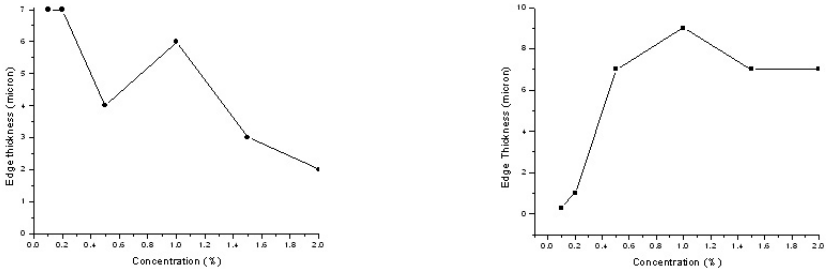

(a) (b)

Figure 38: The edge thickness plotted as a function of the concentration. (a) On hydrophilic surface and (b) on hydrophobic surface.

Anisotropic Distribution: Anisotropy, which is the opposite of isotropy, means that something is directionally dependent. When we are scanning the edge in the two spots of Figure 39, we expect the x-data in spot0 to correspond with the y-data in spot1 for the 1D PSD and vice versa.

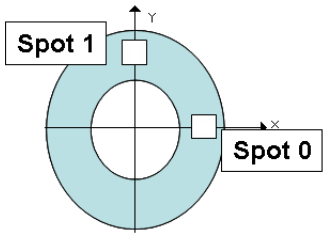

Figure 39: The 1D PSD was measured in two locations.

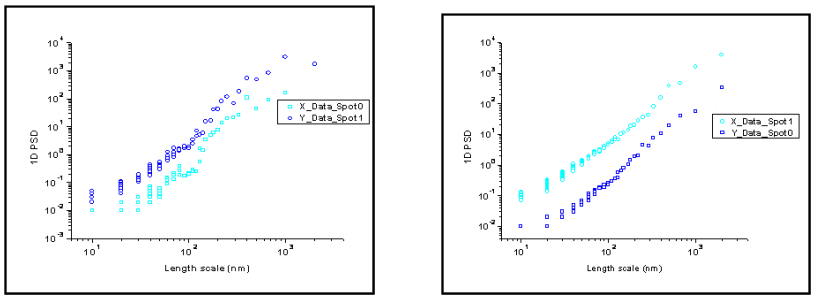

(a) (b)

Figure 40: 1D PSD on the edge for a droplet with concentration 0.1% on a hydrophilic surface.

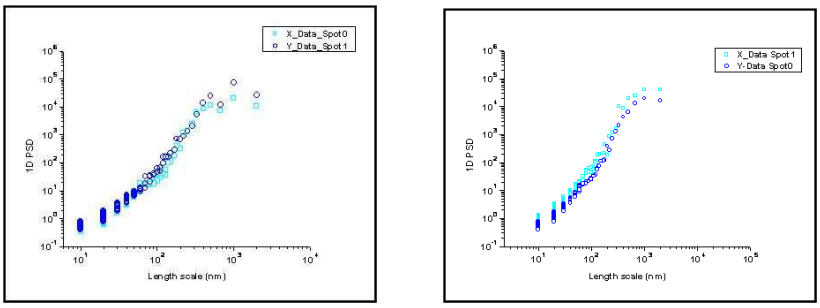

(a) (b)

Figure 41: 1D PSD on the edge for a droplet with concentration 0.5% on a hydrophobic surface.

We can see from the Figures 40 and 41 that the x-data in spot0 is similar to the y-data in spot1 and the other way around. It is thus clear that the distribution is anisotropic on the edge.

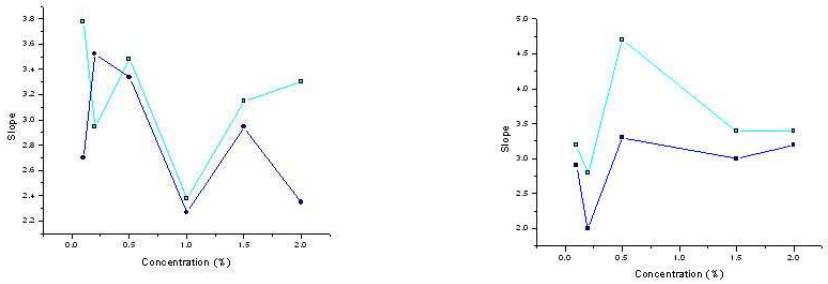

(a) (b)

Figure 42: Slopes as a function of the concentration for (a) hydrophilic glass and (b) hydrophobic glass.

Like for the edge, the inside if the droplets are also influenced by the concentration. This is evident from Figure 42 where the slopes are plotted against the different concentrations.

5.3.4 Diameter and Mass

For the evaporation under the optical microscope we can clearly see that the diameter has decreased with almost 40%, from 1350 μm to 830 μm, 10 minutes after the disposal (see Figure 43). The weight, however, has been reduced with 80% after 10 minutes, from $\sim 10^{-3}$ to $2{\cdot}10^{-4}$. This is evident from Figures 44 and 45.

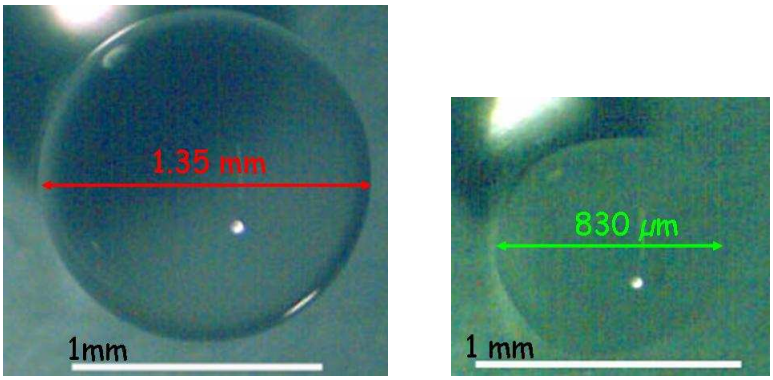

(a) (b)

Figure 43: The evaporation of a droplet seen through an optical microscope. (a) t=0 and (b) t=600 s.

While there is no change in the diameter of the droplet after about 600 seconds, the weight is still changing for another 400 seconds. The edge of the hydrophobic droplet is getting pinned after the collapse, while it continues to evaporate. This is according to the coffee stain effect for wetting substrates.

As seen in Figure 45 the mass is decreasing linearly to begin with, and then it is flattening out. This might be an indication of gelling in the drop as the water is evaporating and the particle density is increasing. According to the datasheet (Appendix A) the gelling is supposed to occur at a concentration of 2% for Laponite RD. From Figure 45 it looks like this gelling is occurring for lower concentrations, at about 0.7%.

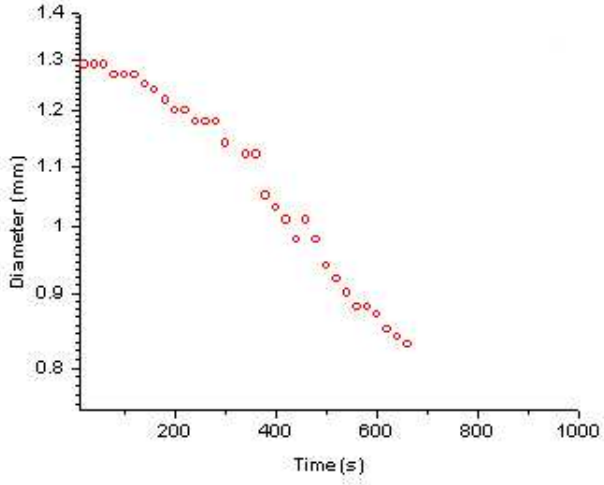

Figure 44: The diameter plotted versus time.

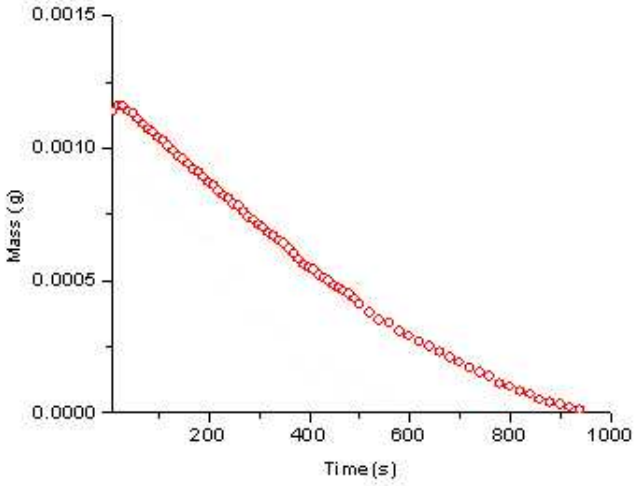

Figure 45: The mass plotted versus time.

6 Conclusion

The intention of this project was to study particle distributions of evaporated droplets, initially containing a certain concentration of the synthetic clay Laponite. This was done by disposing droplets on different substrates for evaporation, in ambient temperature and at 120°C. The surfaces were first studied with an optical microscope and an AFM (contact- and tapping mode), and secondly a roughness- and PSD analysis was performed, utilising the AFM software.

The critical parameters in the result were the deposition surfaces, the concentrations, the evaporation process, and what part of the ring which is being studied. As every experiment takes a lot of time, especially with the tapping mode, we have not been able to repeat the experiments for verification. Hence, the uncertainty in the data has not been quantified.

For many surfaces the contact mode may introduce unwanted features on the surface. This is also the case for the droplets. We therefore need a much softer type of scanning. For the Laponite dispersion droplets even the tapping mode can be too harsh, thus it is important to use a weak force. If the contact with the surface is too hard, the sample might be damaged as seen in Figure 46.

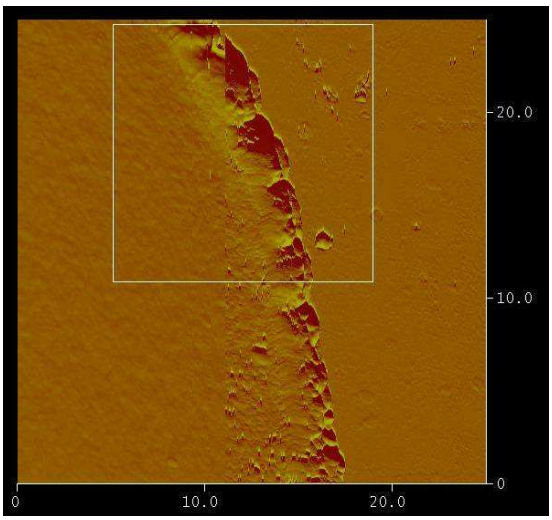

Figure 46: Possible damages caused by the tip, tapping mode with hard contact.

Because the contact mode might be introducing additional features on the surface, the results from the contact mode may not be considered as accurate.

6.1 Suggestions for Future Experiments

For the experiments we tried to study droplets disposed on mica with both the optical microscope and the AFM. However, this proved to be very difficult as it is almost impossible to distinguish the droplet on mica, which is a very hydrophilic surface. Further studies will therefore involve finding a way to make the droplet on mica more visible, and to make the mica hydrophobic.

If possible, the experiments with mass and diameter could be carried out at the same time, i.e. with the balance under the microscope. This in order to check the relation between the diameter and mass of the same drop.

In the future it could also be interesting to study the thermodynamics of the droplets like the water desorption with help from the TGA (Thermal Gravitational Analysis), and the heatcapacity by the use of a DSC (Differential Scanning Calorimetry).

List of Figures

7 Bibliography

References

[1] Eiki Adachi, Antony S. Dimitrov, and Kuniaki Nagayama. Stripe patterns formed on a glass surface during droplet evaporation. *Langmuir*, 11:1057–1060, 1995.

[2] Lars Ramstad Alme. Waxs studies of water transport in a layered synthetic silicate. Master's thesis, NTNU, 2006.

[3] S. W. Bailey. Summary of recommendations of aipea nomenclature committee on clay minerals. *American Mineralogist*, 65:1–7, 1980.

[4] Eric Balnois, Serge Durand-Vidal, and Pierre Levitz. Probing the morphology of laponite clay colloids by atomic force microscopy. *Langmuir*, 2003.

[5] David Baselt. *The tip-sample interaction in atomic force microscopy and its implications for biological applications.* PhD thesis, California Institute of Technology, 1993.

[6] F. Bergaya, B. K. G. Theng, and G. Lagaly, editors. *Handbook of Clay Science.* Elsevier, 2006.

[7] Kaushik Bhattacharya. *Tip Shape and Resolution.* http://mechmat.caltech.edu/∼kaushik/park/3-3-0.htm, California Institute of Technology, 2002.

[8] Thomas J. Bruno, Aneta Lewandowska, Faina Tsvetkov, Keith E. Miller, and Howard J.M. Hanley. Wall-coated open-tubular column chromatography on an organo-clay stationary phase. *Journal of Chromatography A*, pages 143–149, 2002.

[9] Robert D. Deegan. Pattern formation in drying drops. *Physical Review E*, 61(1), 2000.

[10] Robert D. Deegan, Olgica Bakajin, Todd F. Dupont, Greg Huber, Sidney R. Nagel, and Thomas A. Witten. Capillary flow as the cause of ring stains from dried liquid drops. *Nature*, pages 827–830, 1997.

[11] Robert D. Deegan, Olgica Bakajin, Todd F. Dupont, Greg Huber, Sidney R. Nagel, and Thomas A. Witten. Contact line deposits in an evaporating drop. *Physical Review E*, 62(1), 2000.

[12] Digital Instruments Veeco Metrology Group. *MultiMode^{TM} SPM, Instruction Manual, Software Version 4.31ce*, 1996.

[13] Digital Instruments, Veeco Metrology Group. *Support note No. 290, Rev. C, Guidelines for Fluid Operation with a MultiMode AFM*, 2001.

[14] Digital Instruments/Veeco Metrology Group, Inc. *Command Reference Manual, Software Version 5.12rb*, 2001.

[15] J. O. Fossum, H. H. Bergene, Alex Hansen, B. O'Rourke, and G. Manificat. Self-affine crossover length in a layered silicate deposit. *Physical Review E*, 69(036108), 2004.

[16] Jon Otto Fossum. Physical phenomena in clays. *Physica A*, 270:270–277, 1999.

[17] Hua Hu and Ronald G. Larson. Marangoni effect reverses coffee-ring depositions. *The Journal of Physical Chemistry B*, pages 7090–7094, 2006.

[18] Rolf E. Hummel. *Understanding Materials Science, History · Properties · Applications*. Springer, 2004.

[19] Rolf E. Hummel. *Electronic Properties of Materials*. Springer, 2005.

[20] Amethyst Galleries Inc. The clay mineral group. http://mineral.galleries.com/minerals/silicate/clays.htm, 1995.

[21] Veeco Instruments. MMTMEC: Fluid Cell - Tapping Electrochemistry. http://www.veecoprobes.com/accessory_detail.asp?ClassID=215.

[22] Hong-Qiang Li. AFM Resolution. http://www.chembio.uoguelph.ca/educmat/chm729/afm/resolution.htm, Department of Chemistry, University of Guelph, 1997.

[23] A. Mourchid, E. Lécolier, H. Van Damme, and P. Levitz. On viscoelastic, birefringent, and swelling properties of laponite clay suspensions: Revisited phase diagram. *Langmuir*, pages 4718 – 4723, 1998.

[24] Pacific Nanotechnology. *Resolution in an atomic force microscope*. http://www.pacificnanotech.com/afm-tutorial_resolution-in-an-atomic-force-microscope.html, 2006.

[25] Kanak P. S. Parmar. *Oil dispersions of nanolayered silicates in an external electric field: An experimental study*. PhD thesis, NTNU, 2006.

[26] Emil J. Samuelsen. Materials physics, structure, diffraction, imaging and spectroscopy, 2004.

[27] Noushine Shahidzadeh-Bonn, Salima Rafaï, Aza Azouni, and Daniel Bonn. Evaporating droplets. *Journal of Fluid Mechanics*, pages 307–313, 2006.

[28] Leonid Shmuylovich, Amy Q. Shen, and Howard A. Stone. Surface morphology of drying latex films: Multiple ring formation. *Langmuir*, pages 3441–3445, 2002.

[29] Eric Sultan, Arezki Boudaoud, and Martine Ben Amar. Evaporation of a thin film: diffusion of the vapour and marangoni instabilities. *Journal of Fluid Mechanics*, pages 183–202, 2005.

[30] N. Vandewalle, Hendrik Monard, and J. G. McInerney. Physics of droplets, 2006. Proposal for a new COST Action, 165th CSO meeting 27-28 June 2006.

[31] Veeco. Metrology & Instrumentation : AFM / SPM, MultiMode. http://www.veeco.com/products/details.php?pid=177.

[32] Veeco Instruments Inc. *Nanoscope 6.11, Software, User's Guide*, 2003.

[33] Veeco Instruments Inc. *Scanning Probe Microscopy, Training Notebook, Software Version 3.0*, 2003.

[34] Veeco Probes. *Probes and Accessories*, 2006.

[35] B Velde. *CLAY MINERALS, A Physico-Chemical Explanation of their Occurence*. Elsevier, 1985.

[36] Wikipedia. *Atomic force microscope*. http://en.wikipedia.org/wiki/Atomic_force_microscope, 2006.

[37] Wikipedia. Clay. http://en.wikipedia.org/wiki/Clay, 2006.

[38] Wikipedia. Clay minerals. http://en.wikipedia.org/wiki/Clay_minerals, 2006.

[39] Jun Xu, Jianfeng Xia, Suck Won Hong, Zhiqun Lin, Feng Qiu, and Yuliang Yang. Self-assembly of gradient concentric rings via solvent evaporation from a capillary bridge. *Physical Review Letters*, 96(066104), 2006.

[40] A.L. Yarin, J.B. Szczech, C.M. Megaridis, J. Zhang, and D.R. Gamota. Lines of dense nanoparticle colloidal suspensions evaporating on a flat surface: Formation of non-uniform dried deposits. *Journal of Colloid and Interface Science*, pages 343–354, 2006.

A Laponite Data Sheets

ROCKWOOD ADDITIVES LIMITED / ROCKWOOD CLAY ADDITIVES GMBH

PRODUCT BULLETIN/Laponite®

WWW.LAPONITE.COM

Laponite RDS

Description

Laponite RDS is a synthetic layered silicate incorporating an inorganic polyphosphate peptiser. It hydrates and swells in water to give clear and colourless colloidal dispersions of low viscosity known as sols. At 10% concentration in water, these will remain free flowing for 24 hours. On addition of small quantities of electrolyte, highly thixotropic gels are formed rapidly.

Application

Laponite RDS may be utilised as a predispersed liquid concentrate and added to formulations at any point during manufacture. It is used to impart a shear sensitive structure to a wide range of waterborne formulations including household and industrial surface coatings, cleansers, agrochemical and horticultural products.

Typical Characteristics

Property	
Appearance	free flowing white powder
Bulk Density	1000 kg/m^3
Surface Area (BET)	330 m^2/g
pH (2% suspension)	9.7

Chemical Composition (dry basis)	
SiO_2	54.5%
MgO	26.0%
Li_2O	0.8%
Na_2O	5.6%
P_2O_5	4.4%
Loss on Ignition	8.0%

General Specifications

Property	Specification	Rockwood QA Test Code
Sol Stability	Fluid after 24 hours	ELP-L-2B
Sieve Analysis	2% Max >250 microns	ELP-L-6A
Free Moisture	10% Max	ELP-L-5A
Specifications can be agreed to meet individual requirements.		

Storage

Laponite products are hygroscopic and should be stored under dry conditions.

Southern Clay Products, Inc., Rockwood Additives Limited and Rockwood Clay Additives GmbH are wholly owned subsidiaries of Rockwood Specialties Group, Inc.

Rockwood Additives Limited
Moorfield Road Widnes
Cheshire UK WA8 3AA
Tel: +44 (0)151 495 2222 Fax: +44 (0)151 420 4401

Rockwood Clay Additives GmbH
Stadtwaldstr. 44
85368 Moosburg, Germany
Tel: +49 (0) 8761 72 150-0 Fax: +49 (0) 8761 72 150-334

Rockwood Specialties (Singapore) Pte. Limited
171 Chin Swee Road
Unit No: #10-08 San Centre Singapore 169877
Tel: +65 6532 0676 Fax: +65 6532 0502

ROCKWOOD ADDITIVES LIMITED / ROCKWOOD CLAY ADDITIVES GMBH

PRODUCT BULLETIN/Laponite®

WWW.LAPONITE.COM

Laponite RD

Description

Laponite RD is a synthetic layered silicate. It is insoluble in water but hydrates and swells to give clear and colourless colloidal dispersions. At concentrations of 2% or greater in water, highly thixotropic gels can be produced.

Application

Used for imparting a shear sensitive structure to a wide range of waterborne formulations. These include household and industrial surface coatings, cleansers, ceramic glazes, agrochemical, oilfield and horticultural products.

Typical Characteristics

Property	
Appearance	free flowing white powder
Bulk Density	1000 kg/m^3
Surface Area (BET)	370 m^2/g
pH (2% suspension)	9.8

Chemical Composition (dry basis)	
SiO_2	59.5%
MgO	27.5%
Li_2O	0.8%
Na_2O	2.8%
Loss on Ignition	8.2%

General Specifications

Property	Specification	Rockwood QA Test Code
Gel strength	22g min	ELP-L-1H
Sieve Analysis	2% Max >250 microns	ELP-L-6A
Free Moisture	10% Max	ELP-L-5A
Specifications can be agreed to meet individual requirements.		

Storage

Laponite products are hygroscopic and should be stored under dry conditions.

Southern Clay Products, Inc., Rockwood Additives Limited and Rockwood Clay Additives GmbH are wholly owned subsidiaries of Rockwood Specialties Group, Inc.

Rockwood Additives Limited
Moorfield Road Widnes
Cheshire UK WA8 3AA
Tel: +44 (0)151 495 2222 Fax: +44 (0)151 420 4401

Rockwood Clay Additives GmbH
Stadtwaldstr. 44
85368 Moosburg, Germany
Tel: +49 (0) 8761 72 150-0 Fax: +49 (0) 8761 72 150-334

Rockwood Specialties (Singapore) Pte. Limited
171 Chin Swee Road
Unit No: #10-08 San Centre Singapore 169877
Tel: +65 6532 0676 Fax: +65 6532 0502

B Probes for the AFM

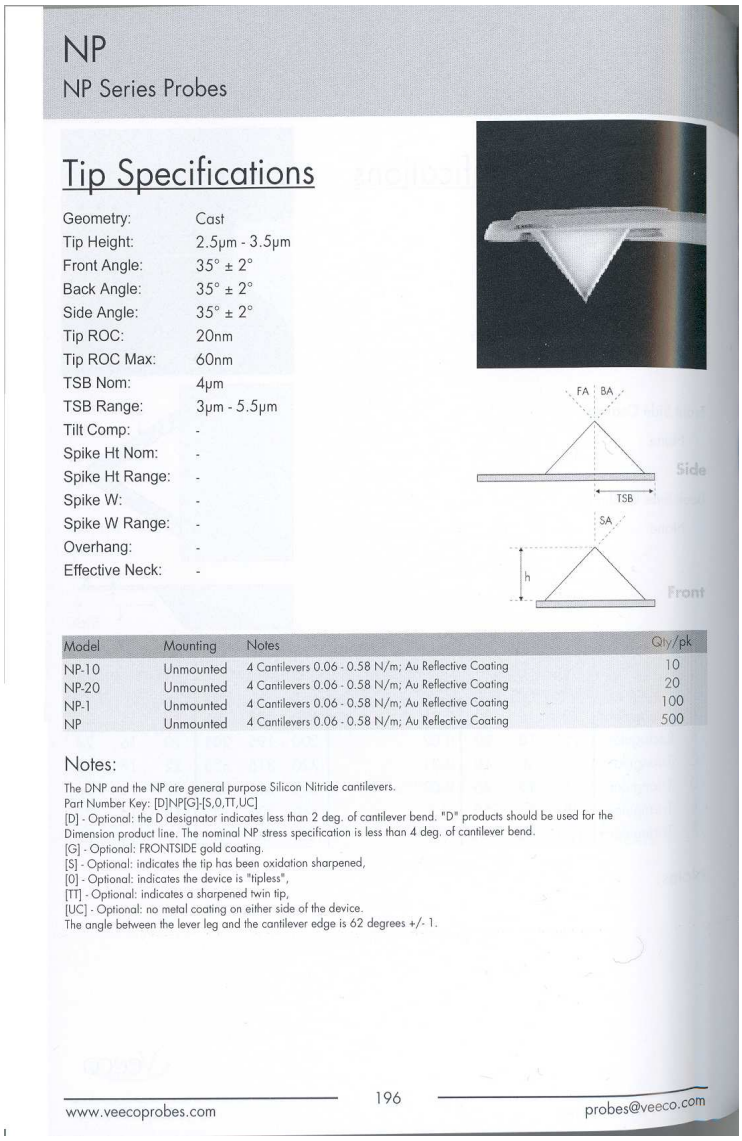

NP

NP Series Probes

Tip Specifications

Geometry:	Cast
Tip Height:	2.5µm - 3.5µm
Front Angle:	35° ± 2°
Back Angle:	35° ± 2°
Side Angle:	35° ± 2°
Tip ROC:	20nm
Tip ROC Max:	60nm
TSB Nom:	4µm
TSB Range:	3µm - 5.5µm
Tilt Comp:	-
Spike Ht Nom:	-
Spike Ht Range:	-
Spike W:	-
Spike W Range:	-
Overhang:	-
Effective Neck:	-

Model	Mounting	Notes	Qty/pk
NP-10	Unmounted	4 Cantilevers 0.06 - 0.58 N/m; Au Reflective Coating	10
NP-20	Unmounted	4 Cantilevers 0.06 - 0.58 N/m; Au Reflective Coating	20
NP-1	Unmounted	4 Cantilevers 0.06 - 0.58 N/m; Au Reflective Coating	100
NP	Unmounted	4 Cantilevers 0.06 - 0.58 N/m; Au Reflective Coating	500

Notes:

The DNP and the NP are general purpose Silicon Nitride cantilevers.
Part Number Key: [D]NP[G]-[S,0,TT,UC]
[D] - Optional: the D designator indicates less than 2 deg. of cantilever bend. "D" products should be used for the Dimension product line. The nominal NP stress specification is less than 4 deg. of cantilever bend.
[G] - Optional: FRONTSIDE gold coating.
[S] - Optional: indicates the tip has been oxidation sharpened,
[0] - Optional: indicates the device is "tipless",
[TT] - Optional: indicates a sharpened twin tip,
[UC] - Optional: no metal coating on either side of the device.
The angle between the lever leg and the cantilever edge is 62 degrees +/- 1.

Figure 47: Tip specifications for contact mode.

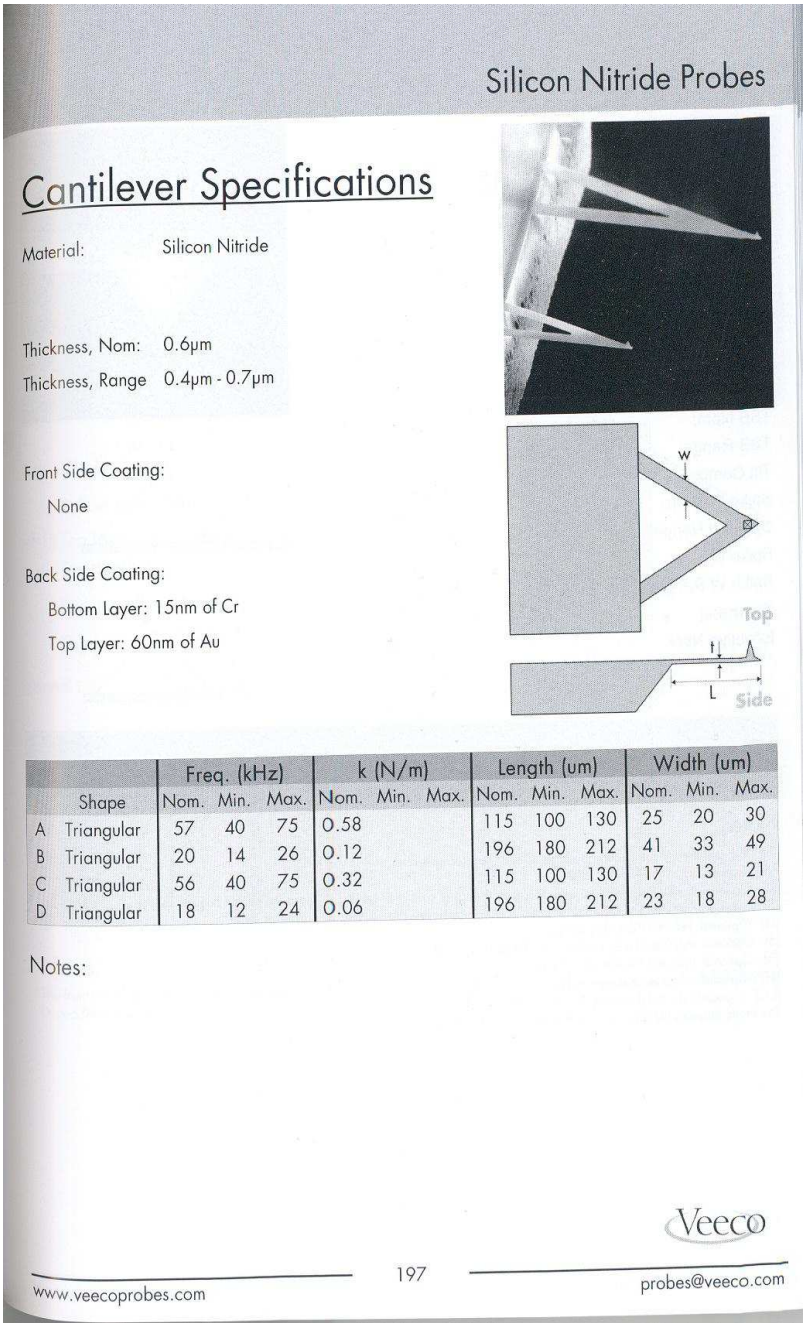

Silicon Nitride Probes

Cantilever Specifications

Material: Silicon Nitride

Thickness, Nom: 0.6μm

Thickness, Range 0.4μm - 0.7μm

Front Side Coating:

None

Back Side Coating:

Bottom Layer: 15nm of Cr

Top Layer: 60nm of Au

	Shape	Freq. (kHz) Nom.	Min.	Max.	k (N/m) Nom.	Min.	Max.	Length (um) Nom.	Min.	Max.	Width (um) Nom.	Min.	Max.
A	Triangular	57	40	75	0.58			115	100	130	25	20	30
B	Triangular	20	14	26	0.12			196	180	212	41	33	49
C	Triangular	56	40	75	0.32			115	100	130	17	13	21
D	Triangular	18	12	24	0.06			196	180	212	23	18	28

Notes:

Veeco

Figure 48: Cantilever specifications for contact mode.

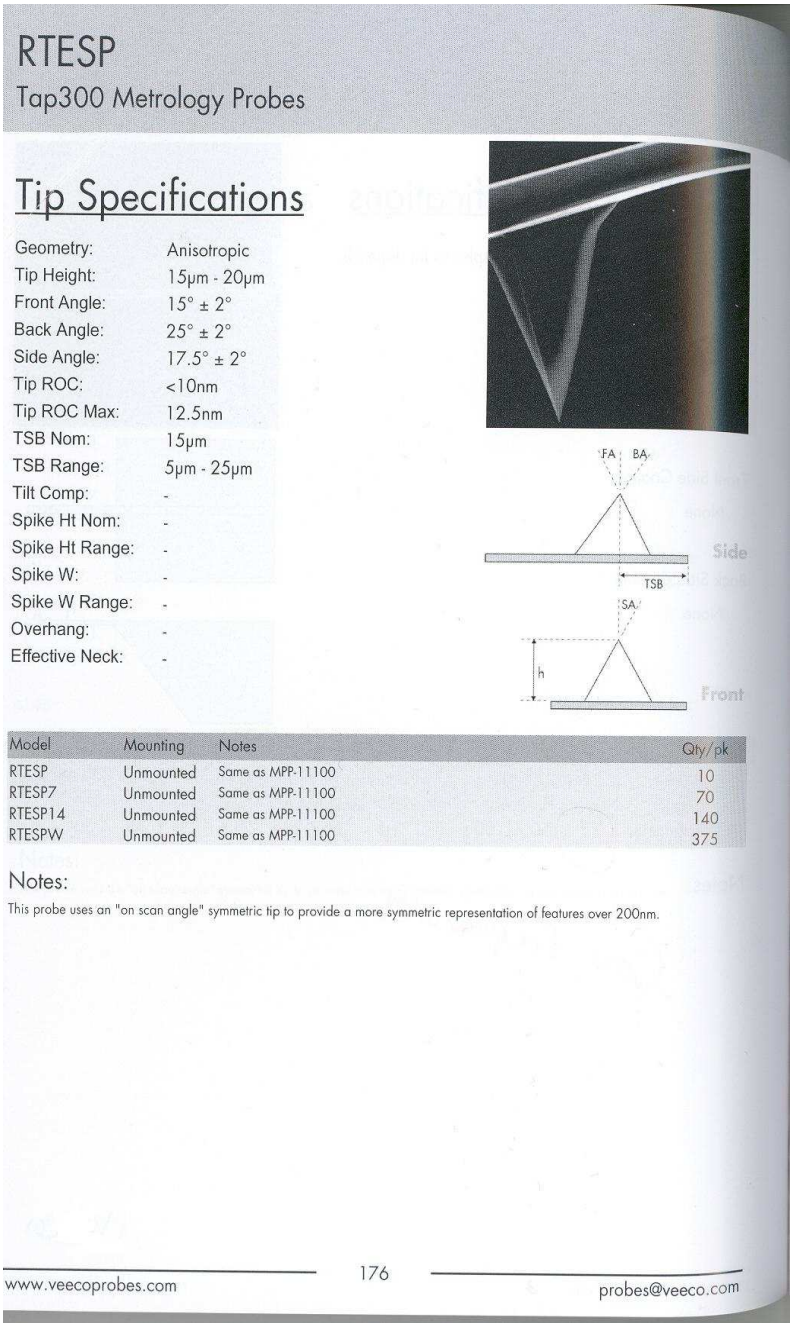

RTESP

Tap300 Metrology Probes

Tip Specifications

Geometry:	Anisotropic
Tip Height:	15µm - 20µm
Front Angle:	15° ± 2°
Back Angle:	25° ± 2°
Side Angle:	17.5° ± 2°
Tip ROC:	<10nm
Tip ROC Max:	12.5nm
TSB Nom:	15µm
TSB Range:	5µm - 25µm
Tilt Comp:	-
Spike Ht Nom:	-
Spike Ht Range:	-
Spike W:	-
Spike W Range:	-
Overhang:	-
Effective Neck:	-

Model	Mounting	Notes	Qty/pk
RTESP	Unmounted	Same as MPP-11100	10
RTESP7	Unmounted	Same as MPP-11100	70
RTESP14	Unmounted	Same as MPP-11100	140
RTESPW	Unmounted	Same as MPP-11100	375

Notes:

This probe uses an "on scan angle" symmetric tip to provide a more symmetric representation of features over 200nm.

Figure 49: Tip specifications for tapping mode.

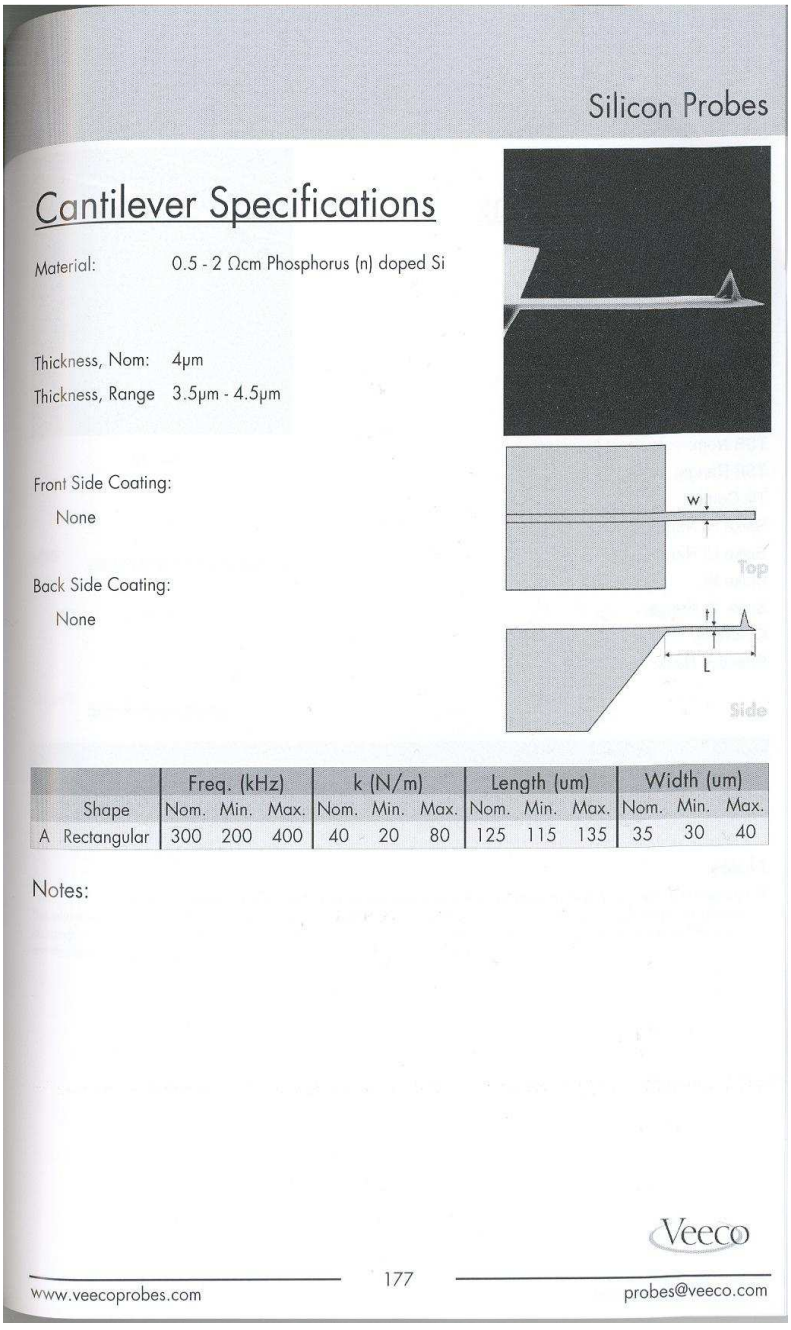

Silicon Probes

Cantilever Specifications

Material: 0.5 - 2 Ωcm Phosphorus (n) doped Si

Thickness, Nom: 4μm

Thickness, Range 3.5μm - 4.5μm

Front Side Coating:

None

Back Side Coating:

None

	Shape	Freq. (kHz) Nom.	Min.	Max.	k (N/m) Nom.	Min.	Max.	Length (um) Nom.	Min.	Max.	Width (um) Nom.	Min.	Max.
A	Rectangular	300	200	400	40	20	80	125	115	135	35	30	40

Notes:

Veeco

www.veecoprobes.com probes@veeco.com

Figure 50: Cantilever specifications for tapping mode.